[American Journal of Science, Vol. 302, April, 2002, P. 312–345]

EXPERIMENTAL INVESTIGATION OF THE KINETICS OF THE REACTION WOLLASTONITE + CALCITE + ANORTHITE = GROSSULAR + CO_2

RALF MILKE* and PAUL METZ**

Institut für Mineralogie, Petrologie und Geochemie der Universität Tübingen
Wilhelmstrasse 56, D-72074 Tübingen, Germany

ABSTRACT. Mechanisms and kinetics of the reaction wollastonite + calcite + anorthite ⇒ grossular + carbon dioxide were studied in powder experiments in the presence of a H_2O-CO_2 fluid with 8 to 13 mole percent CO_2 at 665° to 750°C and 400 MPa. The reaction was studied in terms of overall reaction rates, nucleation rates, and crystal growth rates. Grossular was the only solid reaction product. The crystals were grown around minute andradite-rich cores, which enriched the grossular with traces of iron. At a given temperature, the conversion to grossular + CO_2 increased linearly with time at least up to 25 percent. Reaction rates increased in the temperature range from 710° to 750°C by a factor of 22. At the constant temperature of 730°C the reaction rate increased by a factor of 2.4 when overstepping of the equilibrium temperature was increased from 55° to 95°C due to a decrease in the CO_2-concentration in the fluid.

Nucleation and growth rates were measured at 730°C as a function of time. There was a sharp nucleation rate maximum during the second day of the experiments followed by a steady state nucleation rate at a much lower level during the rest of the experiment. Crystal growth rates permanently decreased either with respect to diameter, surface area, or volume. In experiments with varied surface area for either the reactants or for the grossular, no consistent relationship between surface area and reaction rate was found and thus no single rate-limiting step could be identified.

For the rate-controlling process of the overall reaction a model similar to competitive, diffusion-controlled growth of garnet porphyroblasts is suggested. In this model each grossular crystal is surrounded by a diffusion halo where nutrients deplete with time. Once the diffusion halos impinge throughout the reactant mixture, the diffusion gradients are leveled. Consequently, the nucleation rate drops down to a steady state level and crystal growth rates decrease. Nucleation never totally ceases because the nucleation barrier is overcome by enrichment of andradite component in the garnet cores. Analog enrichment of trace elements during nucleation might be common in metamorphic crystallization. The results achieved will serve to better understand garnet formation in porphyroblastic rocks.

INTRODUCTION

During metamorphism unstable mineral assemblages transform into new crystals and microstructures. The direction of these processes is towards thermodynamic equilibrium. However, often this goal cannot be reached due to kinetic reasons, because of fast fluid flow, slow diffusion, or sluggish nucleation. In some metamorphic structures, the failure to reach equilibrium is obvious; for example where compositional zoning of minerals occurs or reaction rims separate incompatible phases. However, crystallization far from equilibrium might be more common in metamorphism than previously assumed. Numerical modeling has shown that many mineral assemblages and textures might be explained by steady state crystallization far from equilibrium conditions as well as by reaction close to equilibrium (Lasaga and others, 2000, 2001).

Numerical modeling of rocks undergoing metamorphism is dependent on the availability of experimental data on reaction rates and the identification of the

*Also at GeoForschungsZentrum Potsdam, Division 4, Telegrafenberg, D-14473 Potsdam, Germany
**Present address: Hinsiekweg 11 A, D-31061 Alfeld/Leine, Germany

rate-limiting processes. Experimental work on mechanisms and kinetics of metamorphic reactions has shown that in the presence of water, reactions involved in metamorphism occur by dissolution-crystallization mechanisms (Matthews, 1985; Heinrich and others, 1986, 1989; Lüttge and Metz, 1991, 1993). Reaction kinetics are controlled by interface or transport processes, including dissolution (Dachs and Metz, 1988; Winkler and Lüttge, 1999), crystal growth (Schramke and others, 1987; Ostapenko and others, 1991, 1992), and diffusion through reaction rims (Kridelbaugh, 1973; Tanner and others, 1985; Yund, 1997; Liu and others, 1997; Milke and Heinrich, 2002). Other rate-controlling processes are possible, like diffusion through a rock matrix or fluid phase. The rate-limiting reaction step may change during the course of a reaction (Lüttge and Metz, 1991; Lüttge and others, 1998).

In this paper, experimental results are presented on the mechanism and kinetics of the reaction

$$1 \text{ calcite} + 1 \text{ wollastonite} + 1 \text{ anorthite} = 1 \text{ grossular} + 1\ CO_2 \qquad (1)$$

Reaction rates and nucleation and growth rates of grossular were measured. It was also the aim of this study to decipher which processes control the overall reaction rates, as well as the rates of the underlying processes of nucleation and growth. Reaction (1) occurs on the water-rich side of the system CAS-HC ($CaO—Al_2O_3—SiO_2—H_2O—CO_2$), which represents a simplified model composition of marls and calc-silicates (fig. 1). Pioneer experimental studies on reaction mechanisms and kinetics in this system focused on reactions producing or consuming zoisite and anorthite (Allen and Fawcett, 1982; Matthews and Goldsmith, 1984; Matthews, 1985). In these studies, the formation of zoisite from anorthite ± calcite + H_2O was interpreted to be controlled by the dissolution rate of anorthite. In pure water or water-rich fluids, the dissolution of anorthite was incongruent, leading to metastable precipitation of aluminous phases like margarite and mullite.

The present experimental study is the first one addressing a grossular forming reaction in the system CAS-HC. Formation of grossular, as a member of the garnet group, is of particular petrologic interest, since garnets are among the principal alumino-silicate minerals in metamorphic rocks. The tendency for grossular to form porphyroblasts has long been used in field-petrologic studies on metamorphic rocks, to infer rate laws for nucleation and growth from crystal size distributions and chemical zoning of the crystals (Galwey and Jones, 1963, 1966; Jones and Galwey, 1966; Kretz, 1966, 1973, 1974, 1993; Edmunds and Atherton, 1971; Cashman and Ferry, 1988; Carlson, 1989; Carlson and others, 1995; Skelton, 1997; Chernoff and Carlson, 1997). Studies in several metamorphic terranes indicate that garnet growth rates were controlled by the diffusion of dissolved species in the intergranular fluid of the surrounding rock (Carlson, 1989; Carlson, 1991; Denison and Carlson, 1997a, 1997b; Chernoff and Carlson, 1997), whereas others indicate that growth rates were controlled by the garnet surface area (Kretz, 1973, 1993; Daniel and Spear, 1999). It is not clear, which factors in metamorphic garnet crystallization lead to either diffusion- or interface-controlled growth kinetics, as there is generally little information about the rates and mechanisms of intergranular diffusion during metamorphism as well as about garnet growth rates under the conditions of interest.

The interpretation of crystal size distributions and related textural data in metamorphic rocks is essentially based on models which include vaguely constrained factors and functions, like heating rates; rate laws and activation energies for nucleation and growth; rates and activation energies for intergranular diffusion; inhomogeneities in the rocks; as well as the intergranular fluid distribution. By experimental measurement of nucleation and growth rates, our study explores the evolution of

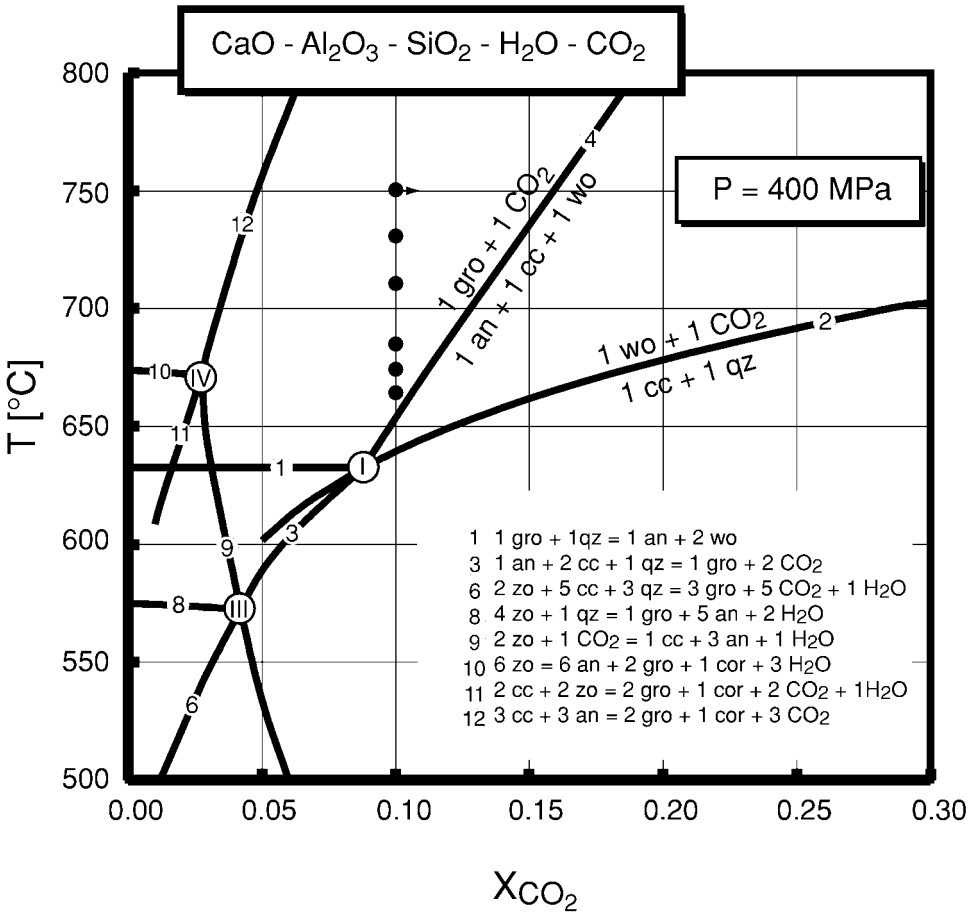

Fig. 1. Water-rich side of the isobaric T—X(CO_2)-diagram of the system CAS-HC at 400 MPa. The curves are calculated using the data set of Gottschalk (1997). The dots indicate the starting conditions for the runs at 710, 730, and 750°C. The arrow marks the X(CO_2)-shift after 10 percent conversion.

crystal size distributions under controlled conditions. In this respect the study represents a bridge between laboratory and field kinetic studies.

STARTING MATERIALS AND EXPERIMENTAL METHODS

Starting materials for the experiments were anorthite from Miyakejima, Japan; wollastonite from Willsboro, New York; and calcite from Iceland. All reactant minerals were analyzed by electron microprobe (EMPA) and found to be chemically homogeneous. Compositions of wollastonite and anorthite are given in table 1. The calcite was the same Iceland spar as used by Dachs and Metz (1988), containing 0.07 wt percent MnO and with MgO and FeO being below the EMPA detection limits. The minerals were crushed from larger crystals and handpicked using a binocular microscope to remove any inclusions of foreign minerals. Grain-size fractions of the starting mixtures were prepared by ultrasonic sieving.

The solids, together with 10.0 mg of H_2O and 9.35 mg of silver oxalate ($Ag_2C_2O_4$), were sealed in gold capsules (20 mm long, ∅ 3 mm) and placed in a drying oven at 110°C for several hours. The rapid decomposition of the silver oxalate at this

TABLE 1

Microprobe analyses in wt percent of wollastonite and anorthite used as starting materials

	Wollastonite Willsboro / U.S.A.[1]	**Anorthite Miyakejima / Japan[2]**
CaO	48.20	18.76
MgO	0.00	0.21
SrO	n. d.	0.06
FeO*	0.39	0.48
MnO	n. d.	n. d.
Al_2O_3	0.01	35.53
SiO_2	51.39	44.36
TiO_2	0.04	n. d.
Cr_2O_3	0.00	n. d.
K_2O	0.02	0.05
Na_2O	0.01	0.47
Σ	100.06	99.92

[1]Average of 10 analyses
[2]Average of 20 analyses
*: total iron as FeO.
n.d. = not determined

temperature yielded 2.7 mg CO_2, thus giving 12.7 mg of a fluid phase consisting of water and carbon dioxide with $X(CO_2) = 0.100 \pm 0.002$. This amount of fluid was generated to avoid crushing of the powder when the capsules were compressed. In standard experiments all reactants were from the size fraction 80–100 μm. The total mass of reactants was 25.4 ± 0.5 mg in stoichiometric proportions relevant to the studied reaction so that the solid : fluid ratio by weight was 2 : 1 at the start of each experiment. The stoichiometry and uniformity of the starting mixture in these experiments provides a starting point in which the varied surface areas of the reactants and the addition of seeds can be compared. Experiments in which the surface area of one reactant was varied were done in three different ways. In the first method (a) the respective reactant was taken from the size fraction 40–60 μm, thereby increasing the surface area of this mineral by a factor of 1.8 and the number of grains by a factor of 6. In the second method (b) all reactants were taken from the 80–100 μm fraction, with one of them being either deficient or in surplus compared to the stoichiometric proportions. Thus, the solid : fluid ratio was not constant, but less or more than 2 : 1, respectively. In the third method (c) again all grains were 80–100 μm with one of the reactants either deficient or in surplus, but the amounts of all three reactants were adjusted in a way such that their total mass was 25.4 ± 0.5 mg. This procedure was followed in order to get a constant solid : fluid ratio of 2 : 1 as in the standard experiments.

Addition of grossular seeds to the starting mixture consisted of substituting a fraction of the reactant mixture with the reaction products from a previous experiment, in which both the amount of the produced grossular and the size distribution of the grossular crystals were known. This reaction mixture was produced in stoichiomet-

ric runs at 730°C for 72 hours. 13 wt percent of this mixture was grossular, the rest was wollastonite, calcite and anorthite in stoichiometric proportions. 83 percent of the grossular crystals were below 20 μm in diameter.

All experiments were carried out in conventional cold-seal pressure vessels with CO_2 as the pressure medium. Temperature was measured with calibrated chromel-alumel thermocouples situated inside the autoclaves in direct contact with the central part of the gold capsule. Pressure was measured by a wire resistance strain gauge with an accuracy of ± 5 MPa. Temperatures for the runs ranged from 665° to 750°C ± 3° at 400 ± 5 MPa. Run durations were varied from 100 minutes to 1826 hours. The heating was performed isobarically at 400 MPa in 30 minutes to run temperature up using a method similar to the fast heating procedure as given by Lüttge and others (1998). Special care was taken to avoid thermal overstepping of the reactions. The stability field of wollastonite (above 640°C at 400 MPa and $X(CO_2) = 0.10$) was reached after 10 minutes of heating. Quenching of the runs was done non-isobarically using compressed air. Pressure was systematically reduced from 400 MPa to 50 MPa during cooling. By this non-isobaric quenching the sample was kept within the stability field of wollastonite down to about 400°C thereby preventing the carbonation of wollastonite during quenching. Cooling took about 90 seconds from 700° to 500°C and about 8 minutes from 700° to 100°C.

The reaction progress was determined from the amount of CO_2 produced. The procedure was as follows. After each run the capsules were weighed and then centrifuged to force the water into one end of the gold tube. Then the tubes were carefully pierced at the other end to let the CO_2 escape and weighed again to determine the amount of carbon dioxide in the capsule. After drying at 110°C for several hours, they were weighed for a third time to determine the water content. The difference in the amount of CO_2 placed in the capsules before the runs and the amount weighed afterwards is the amount of CO_2 produced, which monitors the reaction progress according to the stoichiometry of equation (1). Weighing the water after the runs served as a control because there should be no loss or gain of water. Weighing was performed with a Sartorius MP 8 Ultra Micro Balance with an accuracy of 0.01 mg. The absolute accuracy of the determined reaction progress is within ± 0.5 percent. The solid phases were examined using an optical microscope under crossed polars; a scanning electron microscope (Cambridge Stereoscan 250) with EDX (EDAX 9100); EMPA (ARL SEMQ); and by X-ray powder diffraction. Grossular crystal size distributions were derived by measuring crystal diameters from SEM images in random samples of the run products.

RESULTS

SEM-studies.—Dissolution and growth features are shown on SEM pictures (fig. 2). Morphology suggests that the dissolution of wollastonite and calcite is largely controlled by the different dissolution rates in different lattice directions. The side faces of the wollastonite cleavage prisms are smoothed and show terraces or striations (fig. 2A, B, and C). Etch pits on the prism faces and dissolution channels along the b-axis of the prisms are also present, but as suggested by the dissolution morphology, their impact on total dissolution rates is outweighed by dissolution at surface steps (fig. 2B). In runs below 700°C, that is at low overstepping of the equilibrium temperature, the broken ends of wollastonite prisms evolve into flat crystal faces (fig. 2B). Calcite grains are macroscopically rounded after the experiments, but at higher magnification their surfaces are often stepped by rhombohedral faces in the 100-nm range (fig. 2D). In runs below 700°C, calcite grains disaggregate into numerous sub-crystals, and evolve smooth rhombohedral and rough basis faces {0001} (fig. 2E). Anorthite grains are rounded after the runs. They show no crystallographically determined faces and only rarely four-sided etch pits.

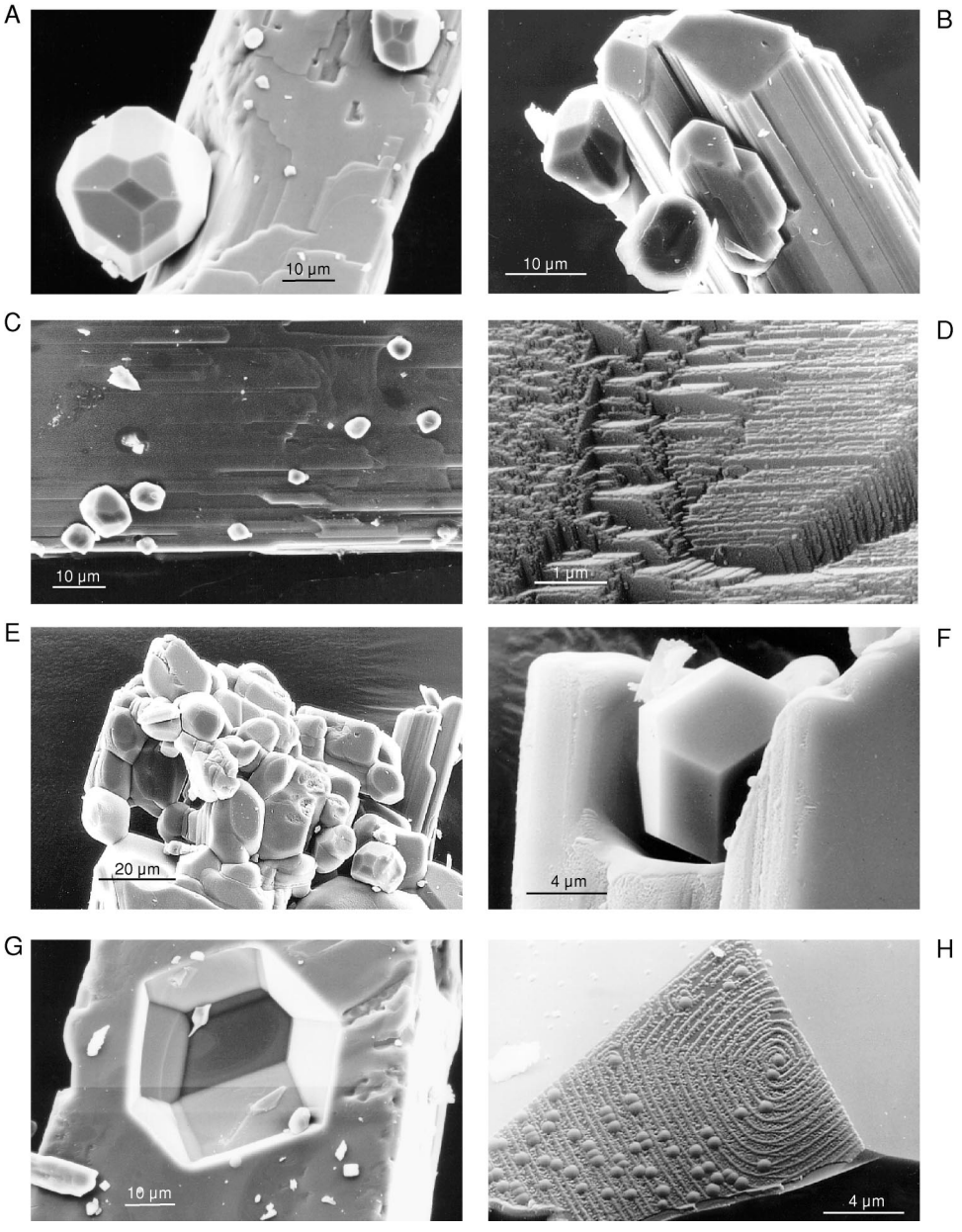

Fig. 2. SEM-micrographs of run products: (A) Grossular crystal in the center of a shallow dissolution embayment in wollastonite after 24 hours. The grossular crystal is a combination of {110} and {211}. G 74 (730°C; 24 h). (B) Flat terminal faces that have formed from broken ends of wollastonite prisms. Grossular crystals indicate that wollastonite was consumed. The formation of flat faces on wollastonite was only observed below 700°C. Note the striation along the wollastonite prisms formed by dissolution. G 17 (685°C; 621 h). (C) Striated surface of a wollastonite prism with numerous small grossular crystals formed at the nucleation rate maximum. G 67 (730°C; 48 h). (D) Calcite surface stepped by rhombohedral faces. Step heights are in the 100 nm range. G 74 (730°C; 24 h). (E) Disaggregation of a calcite grain into subgrains by dissolution parallel to $(10\bar{1}1)$. The edges of subgrains are modified by $(01\bar{1}1)$ and (0001). Subgrain formation due to dissolution was only observed below 700°C. G 17 (685°C; 621 h). (F) Initial crystallization of grossular on wollastonite in a deep dissolution pit. The grossular crystal shows only {110}. Pure dodecahedral grossular and deep leaching of the reactants are only observed in the initial phase of the reaction. G 11 (745°C; 1 h). (G) Imprint of a large grossular crystal plucked out of an anorthite surface. Dissolution and crystallization took place *in-situ*, that is, replacement of anorthite by grossular. G 74 (730°C; 24 h). (H) Growth spiral on (110) of a grossular crystal, decorated by quench-SiO_2. WCAG 6 (695°C; 240 h).

An effective dissolution mechanism was observed in the initial phase of the reaction (run time ≤ 24 hours at 730°C). During this phase of the reaction, dissolution was enhanced in the vicinity of growing grossular crystals, resulting in dissolution embayments (fig. 2A and F). Such embayments appeared on the surfaces of all three reactant minerals. The embayments are deep and narrow after a short run time (fig. 2F), and then evolve into flat halos around the garnet crystals (fig. 2A). After two days, these embayments disappeared. They are not present around grossular crystals that nucleated after the first day of the run (fig. 2C). In 1-day-experiments some of the anorthite surfaces had negative imprints of plucked-out grossular crystals (fig. 2G). In this case, grossular growth is held to have been a replacement reaction where dissolution was coupled with *in-situ* crystallization.

Grossular crystals sat on surfaces of all three reactant phases or overgrew each other. Diameters of most grossular crystals ranged from 5–30 μm with only a few outliers. In the 730°C-experiments, the largest crystals were approximately 50 μm in diameter. A very few crystals of up to 130 μm in diameter were observed in the runs at 675° (run G 18) and 685°C (G 17), where the equilibrium temperature was overstepped by only 20 and 30°C, respectively. At 665°C (G 99), only small crystals formed with sizes of around 10 μm.

Grossular mostly crystallized as combinations of trapezohedron {211} and dodecahedron {110} with {211} crystal shape slightly dominating (fig. 2A). Only in the very beginning of the reaction were pure dodecahedra present (fig. 2F). Growth spirals were observed on {110} and less commonly {211}, where they were outlined by quench-SiO_2 (fig. 2H). Growth spirals occurred in many experiments of variable duration and temperature. This observation indicates that garnet crystallized in the spiral growth regime in every stage of the experiments.

Electron microprobe analyses.—All the garnet crystals contain some iron. The iron comes from the trace iron that occurs in wollastonite and anorthite. Iron is enriched in the core regions of the garnet crystals with diameters <5 μm. Maximum concentrations reach up to 7 wt percent Fe_2O_3, corresponding to 21 mole percent andradite component (table 2). Due to the diameter of the electron beam these are minimum

TABLE 2

Microprobe analyses of garnet crystals of various sizes by wt percent. Run G 33 was 124 hours at 750°C; run G 45 was 168 hours at 710°C

size	**4x4 μm**		**2x2 μm**	**28x28 μm**		**14x12 μm**	
No. position	G33-1.8 center	G33-1.10 margin	G33-5 center	G33 18.10 center	G33-18.2 margin	G45-1 center	G45-1r2 margin
CaO	38.63	39.78	38.43	38.59	37.90	37.35	36.91
Al_2O_3	16.58	20.44	18.85	19.57	22.86	16.23	21.64
SiO_2	40.40	39.41	40.31	38.54	39.73	39.40	42.01
Fe_2O_3*	5.60	0.77	3.66	2.62	0.56	6.74	1.20
S oxides	101.21	100.40	101.25	99.32	101.05	99.72	101.76
compos.	$gro_{82}and_{18}$	$gro_{98}and_{02}$	$gro_{89}and_{11}$	$gro_{92}and_{08}$	$gro_{99}and_{01}$	$gro_{79}and_{21}$	$gro_{97}and_{03}$

*all iron calculated as Fe_2O_3

values. The outer zones of the crystals generally contain ≤ 1 wt percent Fe_2O_3, reflecting the bulk iron content of the reactants (0.4 wt percent FeO, see table 1). EMP analyses were made from crystals synthesized at 710° and 750°C, and andradite-enriched cores were found in both analyses. Although exposure of an Fe-rich core is a product of the sectioning, iron-rich cores were found in 90 percent of the crystals grown at 710°C and 50 percent grown at 750°C. The maximum iron concentrations were identical at both temperatures. Iron-rich cores were found in crystals of all sizes from 2 to 36 μm in diameter. This fact suggests that grossular growth always starts with small Fe-enriched grandite crystals through the entire course of the reaction. Ti, Mg, and Mn were below the microprobe detection limit. The presence of a hydrogrossular component is unlikely above 700°C (Huckenholz and Fehr, 1982). This conclusion is supported by the high totals for oxides in the EMP analyses (~100 wt percent).

Conversion measurements.—Conversion can be monitored by weighing the produced CO_2 as long as no parallel reactions occur and no re-carbonation of reactants occurs during quenching. No solid reaction products except grossular were found in any of the runs. The only parallel reaction that could affect the measurements is non-stoichiometric grossular formation in the very early stages of the experiments, resulting from incongruent dissolution of wollastonite (Casey and others, 1993; Xie and Walther, 1994). If this reaction were to occur to any significant extent, using CO_2 as a monitor would give conversion measurements that are too low. The possible occurrence of this parallel reaction was demonstrated in runs at 710°C and an initial $X(CO_2)$ of 0.10 with only wollastonite and anorthite as starting materials. Although wollastonite + anorthite is a stable assemblage under these conditions, some grossular was produced in these experiments. However, the estimated reaction progress to grossular was well below 1 percent of the reactants, so that any deviation resulting from non-stoichiometric grossular growth would probably be within the error limit of the conversion measurements.

At temperatures below 700°C, the reaction is so slow that laboratory measurements of the reaction rates are hardly practical. For example, at 675°C only 1 percent conversion is attained after 621 h. Conversion versus time curves were determined at temperatures of 710°, 730°, and 750°C. The starting points of the experiments are shown in figure 1 relative to the position of the equilibrium curve for the reaction anorthite + calcite + wollastonite = grossular + carbon dioxide. Results are presented in table 3 and figure 3. The conversions versus time curves allow for a linear fit up to a conversion of about 25 percent. Reaction rates (that is conversion per time) are 0.016 percent per hour (710°C), 0.14 percent per hour (730°C), and 0.35 percent per hour (750°C). Thus, the reaction rate increases by a factor of 22 as the temperature is increased from 710° to 750°C.

When the run temperature is increased, the overstepping of the equilibrium temperature, $\Delta T = T - T_{eq}$, is increased as well and the two effects act simultaneously. A further complication arises from the shift in $X(CO_2)$ as the reaction progresses, which successively decreases the overstepping during the course of a run. For illustration, the arrow in figure 1 at 750°C shows the effect of a 10 percent conversion. The reaction leads to a shift in $X(CO_2)$ from 0.100 to 0.108 and thereby approaches the equilibrium temperature by 14°C. To study the effect of ΔT on the reaction rate, a number of experiments were performed at 730°C with an initial higher and lower $X(CO_2)$ than 0.10 (G 111, G 123, G 124, and G 125 of table 3). Only experiments with conversions from 9 to 12 percent were considered so that the shift in $X(CO_2)$ in all runs was more or less the same and its effect was eliminated. Reaction rates versus $T - T_{eq}$ are shown in figure 4. At the given temperature of 730°C, reaction rates increase with increasing overstepping. The scatter of the data would allow several fitting functions, all of which have to go through zero at $\Delta T = 0$. If the data are tentatively

TABLE 3

Results of the unseeded, stoichiometric experiments

Run No.	T [°C]	t [h]/[d]	React. [mg]	X(CO_2) Start	X(CO_2) End	prod.CO_2 [mg]	prod.CO_2 [µmol]	Conv. [%]	prod.CO_2 per 25.4 mg mixt. [mg]
G 99	665	1826 / 76	25.00	0.100	0.100	„0“	„0“	<1	„0“
G 18	675	621 / 26	39.32	0.098	0.100	0.03	0.7	1	0.02
G 17	685	621 / 26	37.64	0.099	0.099	0.07	1.6	2	0.05
G 45	710	168 / 7	25.13	0.099	0.108	0.07	1.7	3	0.12
G 38	710	335 / 14	25.03	0.099	0.103	0.12	2.8	5	0.07
G 73	710	503 / 21	25.77	0.098	0.105	0.22	5.0	8	0.22
G 75	710	503 / 21	25.08	0.098	0.106	0.21	4.8	9	0.22
G 80	710	672 / 28	25.88	0.100	0.109	0.25	5.6	11	0.24
G 81	710	672 / 28	25.15	0.099	0.106	0.22	4.9	9	0.22
G 27[bq]	730	239 /10	24.52	0.099	ca. 0.120	ca. 0.59	ca. 5.89	ca. 27	0.61
G 37	730	120 / 5	25.45	0.099	0.113	0.40	9.2	17	0.40
G 46	730	73 / 3	25.14	0.090	0.093	0.31	7.0	14	0.31
G 48	730	73 / 3	25.13	0.099	0.108	0.26	6.0	12	0.27
G 52	730	120 / 5	24.79	0.100	0.113	0.37	8.3	16	0.38
G 67	730	48 / 2	25.25	0.100	0.106	0.16	3.7	7	0.16
G 68	730	96 / 4	25.17	0.100	0.111	0.34	7.6	15	0.34
G 69	730	48 / 2	25.06	0.100	0.105	0.14	3.3	6	0.15
G 70	730	96 / 4	25.41	0.100	0.111	0.33	7.5	14	0.33
G 71	730	24 / 1	24.87	0.100	0.103	0.07	1.5	3	0.07
G 72	730	24 / 1	25.13	0.099	0.100	0.03	0.7	1	0.03
G 74	730	24 / 1	25.44	0.099	0.101	0.06	1.4	2	0.06
G 84	730	72 / 3	26.57	0.100	0.105	0.24	5.4	10	0.23
G 86	730	72 / 3	25.80	0.101	0.106	0.21	4.9	9	0.20
G 94	730	120 / 5	25.85	0.100	0.113	0.41	9.2	18	0.40
G 97	730	36 / 1.5	25.26	0.099	0.102	0.10	2.2	4	0.10
G 111	730	84 / 3.5	25,34	0.108	0.116	0.24	5.4	10	0.24
G 120	730	24 / 1	25.22	0.098	0.100	0.07	1.7	3	0.07
G123	730	100 / 4	25.50	0.108	0.116	0.26	6.0	12	0.26
G124	730	100 / 4	25.09	0.112	0.120	0.24	5.3	11	0.24
G125	730	48 / 2	26.24	0.090	0.097	0.28	6.4	10	0.27
G 11	745	1 / -	25.20	0.102	0.102	„0“	„0“	<1	„0“
G 33	750	124 / 5	24.98	0.099	0.121	0.69	15.6	30	0.70
G 34	750	124 / 5	25.04	0.100	0.122	0.68	15.5	30	0.69
G 35	750	74.5 / 3	25.07	0.098	0.119	0.57	13.0	25	0.58
G 36	750	74.5 / 3	25.07	0.099	0.106	0.53	12.1	24	0.54
G 50	750	48.5 / 2	25.16	0.099	0.113	0.40	9.0	18	0.40
G 76	750	42 / 1.75	25.19	0.100	0.115	0.44	10.0	19	0.44
G 77	750	42 / 1.75	26.73	0.100	0.111	0.40	9.1	16	0.38
G 78	750	24 / 1	24.63	0.099	0.107	0.20	4.5	9	0.21

[bq]: blow quench experiment

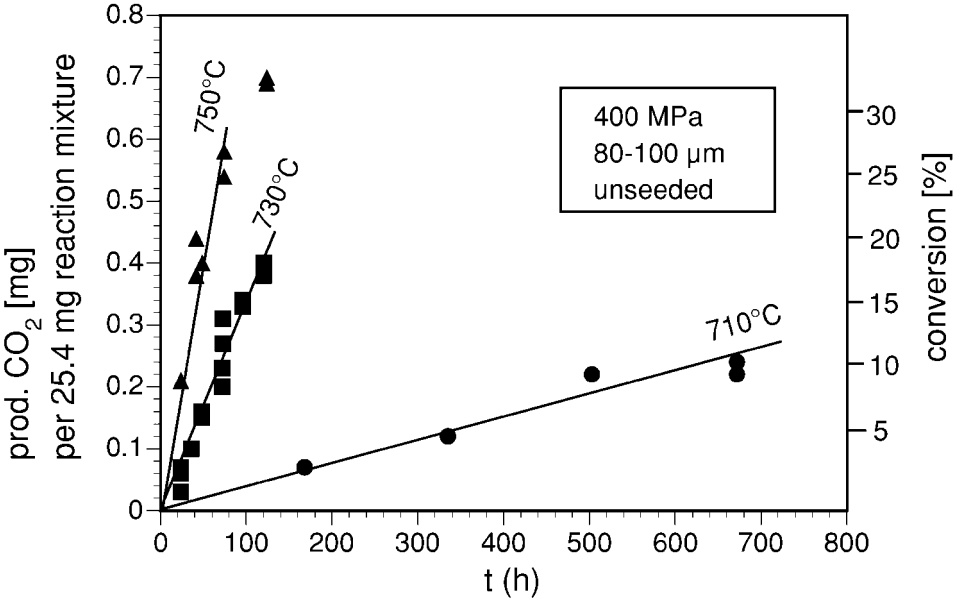

Fig. 3. Conversion versus time in unseeded, stoichiometric experiments at 710°, 730°, and 750°C. Initial $X(CO_2)$ was 0.10 in all runs.

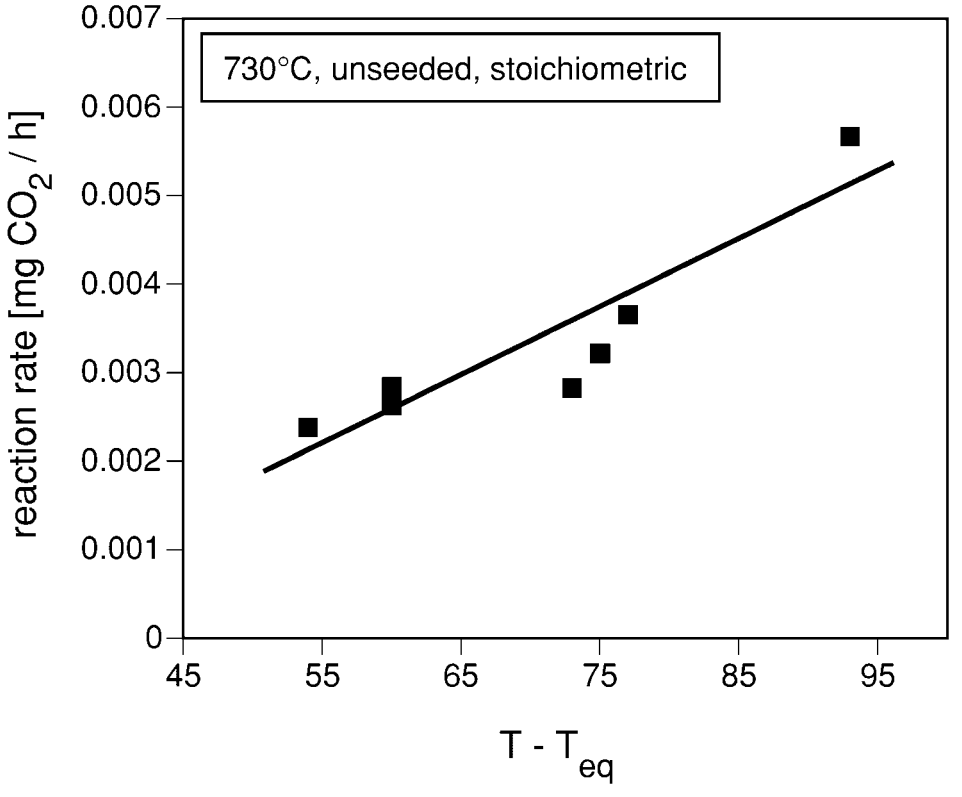

Fig. 4. Reaction rates versus temperature overstepping, $T - T_{eq}$, in unseeded, stoichiometric standard experiments at 730°C with varied initial $X(CO_2)$ between 0.112 and 0.009, corresponding to an overstepping between 54° and 95°C. All experiments went to almost equal conversions between 9 and 12 percent.

TABLE 4

Results of experiments with varied surface areas of the reactants. Surface area was increased by using a smaller grain fraction or a surplus of one reactant, respectively. Decrease of surface area was achieved by a deficiency of one reactant

Experiment No.	n times surface of ...	T [°C]	t [h]/[d]	React. [mg]	$X(CO_2)$ Start	$X(CO_2)$ End	prod. CO_2 [mg]	prod. CO_2 [µmol]
method a)								
G 79	ca.1.8 an	730	72 / 3	24.47	0.100	0.106	0.27	6.2
G 82	ca.1.8 wo	730	72 / 3	25.88	0.099	0.107	0.31	6.9
G 83	ca.1.8 cc	730	72 / 3	25.58	0.098	0.109	0.35	7.9
method b)								
G 91	0.5 wo	730	120 / 5	22.67	0.099	0.111	0.37	8.5
G 95	2 wo	730	120 / 5	31.14	0.099	0.110	0.31	7.0
G 96	2 cc	730	120 / 5	30.34	0.098	0.109	0.31	7.1
G 98	2 an	730	120 / 5	39.45	0.099	0.109	0.34	7.8
method c)								
G 59	1.5 cc	730	120 / 5	25.19	0.099	0.110	0.32	7.2
G 61	1.5 wo	730	120 / 5	25.32	0.100	0.112	0.34	7.7
G 62	2 wo	730	120 / 5	25.27	0.102	0.110	0.24	5.5
G 63	1,5 an	730	120 / 5	25.31	0.099	0.110	0.32	7.2
G 64	2 an	730	120 / 5	24.79	0.098	0.107	0.26	5.8

The surface area of each reactant was varied by three methods in turn:

a) Smaller grains of one reactant (40-60 µm instead of 80-100 µm), increase in surface area c. 1.8 times.

b) Excess/deficiency of one reactant with respect to the stoichiometric standard runs (all grains 80-100 µm); fluid amount held constant at 12.7 mg (10.0 mg H_2O + 2.7 mg CO_2) as in the standard runs, such that the solid-fluid ratio by weight ≠ 2 : 1.

c) Total mass of solids adjusted to 25.4 mg (as in standard runs); fluid amount held constant at 12.7 mg (10.0 mg H_2O + 2.7 mg CO_2), such that the solid-fluid ratio by weight = 2 : 1.

approximated by a linear fit over the $T - T_{eq}$ range of the experiments, the reaction rate increases only by a factor of 2.4 when ΔT is increased by 40°C.

Table 4 and figure 5 show the results for stoichiometric starting mixtures where one reactant was in the grain size range of 40–60 µm and the other two were in the 80–100 µm range. In this case the surface area of the smaller sized phase was enlarged by a factor of 1.8 compared to the standard experiments. The reaction rate was distinctly increased when the surface area of calcite was enlarged. With smaller wollastonite grains the rate was only slightly increased, whereas smaller anorthite grains had no effect on the reaction rate. Results were different when the surface area of one reactant was doubled by the presence of excess grains relative to the stoichiometric mixture, though all grains remained in the 80–100 µm size range. All runs resulted in slower reaction rates compared to the standard runs. Figure 6 demonstrates that reaction rates reached a maximum for stoichiometrically composed mixtures and decreased with increasing deviation from stoichiometry. If one reactant was doubled relative to the stoichiometric mixture, the reaction rates decreased to 65 percent of the

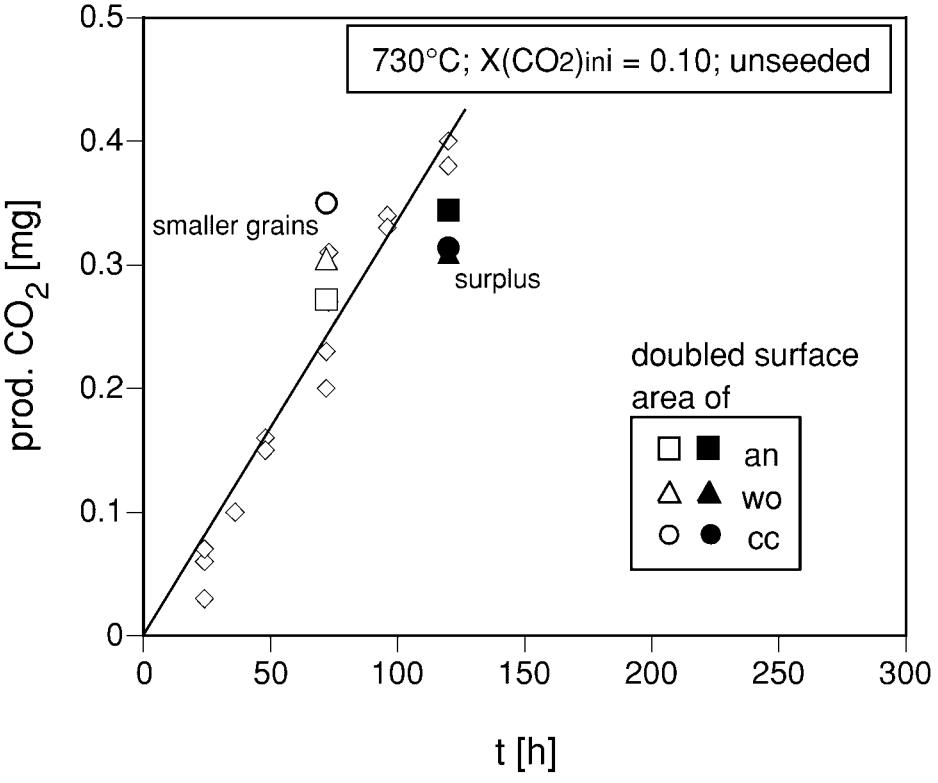

Fig. 5. Conversion (produced CO_2) versus time in runs with doubled surface area of one reactant. Experiments using smaller grains (open symbols) or grain surplus (filled symbols) in comparison to the standard experiments (open rhombs and line from fig. 3). All experiments at 730°C; $X(CO_2)_{ini} = 0.10$.

rates for the stoichiometric mixtures. This trend is identical in all runs, no matter which reactant was added in surplus. When the total amount of solids was increased in method b (surplus of one reactant without adjustment of the fluid amount) the reaction rates were higher than in method c (one reactant doubled yet total mass of reactants kept at 25.4 mg), but still distinctly lower than in the stoichiometric runs (with 25.4 mg of the solids).

When grossular seeds were added to the starting mixtures, the reaction rates were significantly enhanced compared to the unseeded runs (table 5 and fig. 7). In experiments at 710°C, substituting 3, 6, and 9 mg of the reactants with a pre-reacted mixture (corresponding to 0.49, 0.98, and 1.47 mg grossular seeds) resulted in a CO_2 production of 0.9, 1.2, and 2.2 μg CO_2/h, or conversion rates of 0.04, 0.05, and 0.10 percent/h, respectively. These results mean that the rates were 2.2, 2.9, and 5.4 times faster than in unseeded runs. Assuming, as an approximation, a linear relation between reaction rates and the amount of seeds, the rate of CO_2 production increased by 1 μg CO_2/h and the conversion rate by 0.4 percent/h with each mg of grossular seeds (fig. 8).

To study further the effect of grossular seeds on the reaction rate, a special type of run was performed by twice quenching and reheating in one experiment. The experiment started with two capsules in one vessel and the conditions were the same as the standard unseeded experiment at 710°C for 649 hours, except for the two

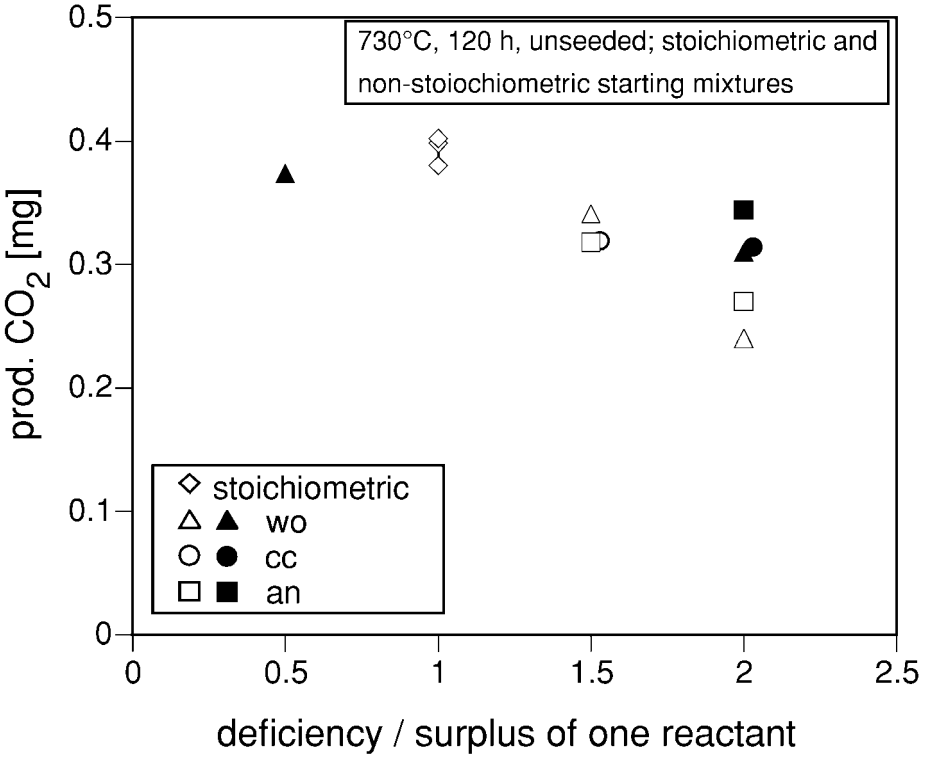

Fig. 6. Conversion (produced CO_2) in runs at 730°C for 120 h ($X(CO_2)_{ini}$ = 01.10) with one reactant in surplus or deficiency compared to the stoichiometric runs. Variation of surface area after method b (filled symbols); after method c (open symbols); stoichiometric experiments (open rhombs). For explanation of methods b and c see text.

interruptions after 168 hours and 335 hours. The grossular crystals already present at the first and second interruptions acted as seed crystals when the vessel was brought under run conditions again. At the first interruption (168 h) both capsules were quenched, left in the vessel, and heated up again. After the second interruption (335 h) one capsule was carefully extracted and the CO_2-production measured while the remaining capsule was heated up again and finally quenched after 649 hours. Results are shown in figure 7 by stars. Using the conditions of the standard experiments, at the first interruption 0.08 mg CO_2 and 0.53 mg grossular were produced. At the second interruption 0.19 mg CO_2 and 1.88 mg grossular had been formed and at the end of the experiment 0.29 mg CO_2 were measured. Within the error range, the reaction rate after each interruption was identical to that in the uninterrupted standard runs at 710°C.

Nucleation rates of grossular.—Nucleation rates were derived by combining the grossular crystal size distributions, based on measured diameters, D_x, with the conversions of the reaction. The method is described in Appendix A.

Grossular nucleation rates were determined from 5 experiments at 730°C with durations from 24 to 239 hours (G 74, G 67, G 48, G 52, and G 27; table 6). The measured crystal size distributions of the grossular crystals are depicted in the histograms in figure 9. The size distribution is nearly symmetric after 24 hours, but positively skewed from 48 to 239 hours. The number of grossular crystals formed in

TABLE 5

Results of seeded runs. Seeding was performed by substituting a fraction of the reactant mixture with the mixture from a previous experiment

Run No.	T [°C]	t [h]/[d]	Reactant mixture[1] [mg]	Pre-react. mix / seeds [mg]	X(CO_2) Start	X(CO_2) End	prod. CO_2 [mg]	prod.CO_2 per 25.4 mg start. mixt. [mg]	Conv [%]
G 142	710	96 / 4	24.70	3.08 / 0.50	0.098	0.101	0.08	0.08	3
G 146	710	240 / 10	25.25	3.03 / 0.49	0.098	0.105	0.22	0.22	10
G 143	710	288 / 12	25.15	3.00 / 0.48	0.097	0.105	0.24	0.24	11
G 144	710	168 / 7	25.95	6.04 / 0.99	0.098	0.105	0.20	0.20	8
G 147	710	240 / 10	25.13	6.00 / 0.98	0.099	0.108	0.27	0.27	12
G 145	710	288 / 12	25.49	6.09 / 0.99	0.099	0.108	0.25	0.25	11
G 148	710	96 / 4	25.26	8.98 / 1.47	0.099	0.106	0.21	0.21	9

[1]: seeds included

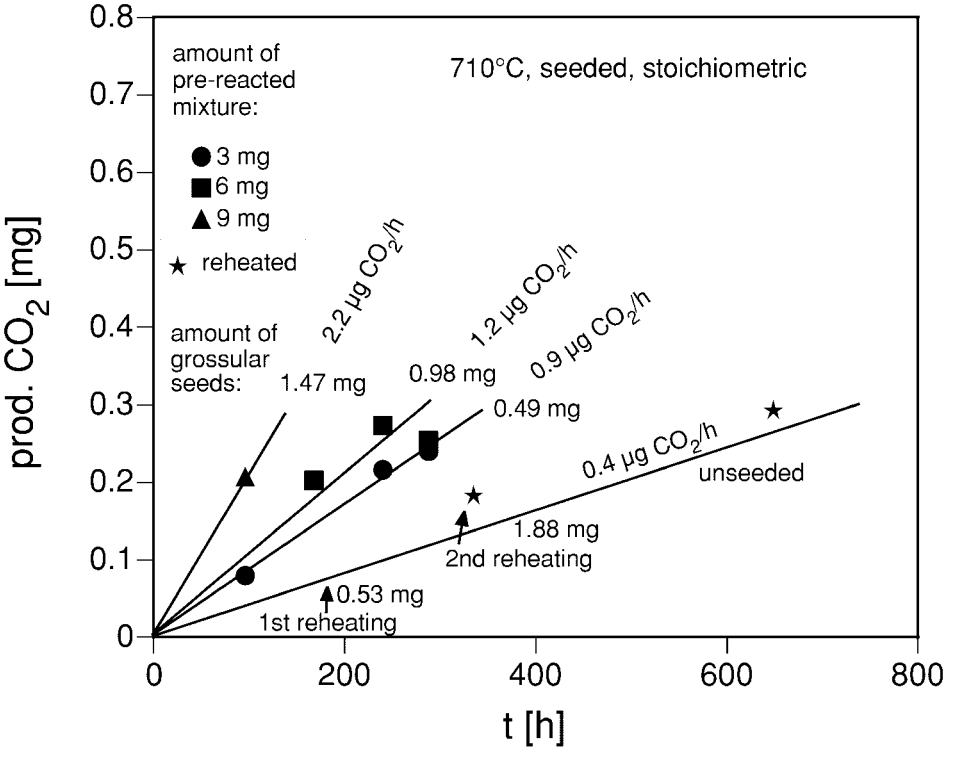

Fig. 7. Conversion (produced CO_2) versus time in seeded experiments (710°C; $X(CO_2)_{ini}$ = 0.10; stoichiometric). Seeding by substitution with 3 mg (●), 6 mg (■), and 9 mg (▲) of pre-reacted mixture, that is, adding of 0.49 mg, 0.98 mg, and 1.47 mg grossular seeds, respectively. Results of the reheating experiment are shown as stars (★). The conversion-time curve for unseeded experiments at identical run conditions from figure 3 is shown as reference line. The numbers give mass of grossular seeds and reaction rates.

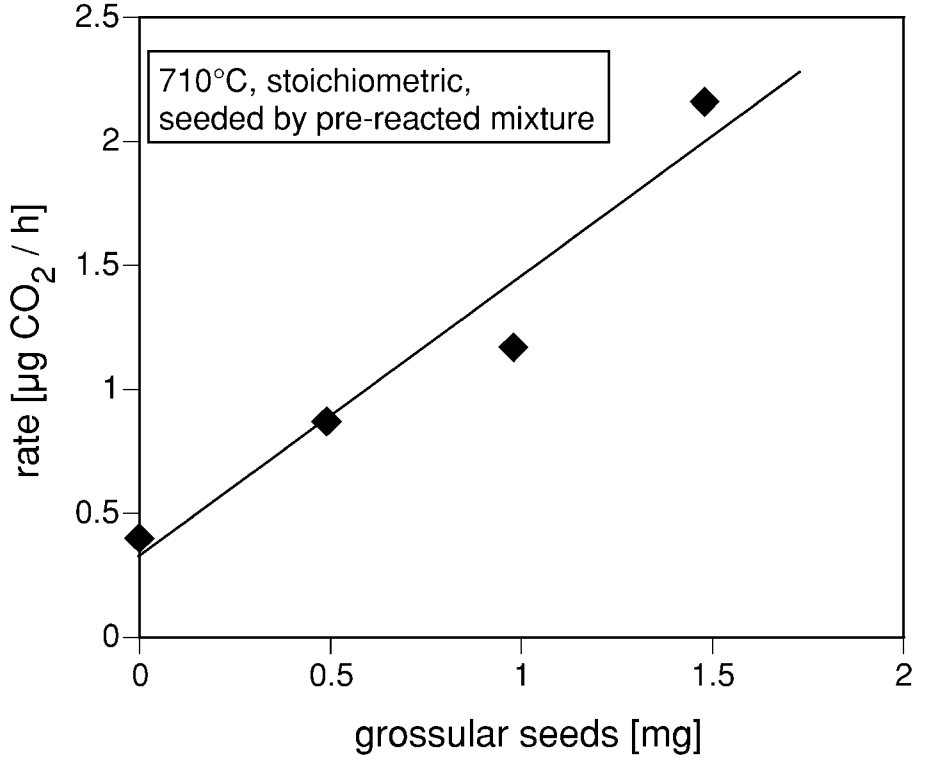

Fig. 8. Reaction rate versus mass of grossular seeds. Data from the unseeded and seeded experiments at 710°C from figures 3 and 7.

each experiment, N_{gro}, is calculated with equation (A2) (Appendix A) and listed in table 6. To make the results of the 5 runs comparable, $N_{V,gro}$, the number of grossular crystals formed in 1 cubic centimeter of solid phases, was calculated with equation (A4). In figure 10A, $N_{V,gro}$ is shown as a function of run time. $N_{V,gro}$ is 0.3×10^7 after 24 hours, then increases rapidly to 4.2×10^7 at 48 hours and then slightly up to 10.3×10^7 after 239 hours. Using equation (A6), the integrated nucleation rate, R_n, was obtained (table 6 and fig. 10B). Nucleation started relatively sluggishly during the first 24 hours of the reaction. A sharp nucleation rate maximum of $\geq$ 450 nuclei cm^{-3} sec^{-1} was attained during the second day of the experiments. Soon after this maximum the nucleation rate dropped down to a steady state rate of about 60–70 nuclei cm^{-3} sec^{-1} for the rest of the experiment up to 239 hours (27 percent conversion).

Nucleation density.—The nucleation density for the heterogeneous nucleation of grossular on the reactant surfaces was determined as the number of garnet crystals grown on the surface of each reactant grains, divided by the geometrical surface area of the reactant. Figure 11 shows the nucleation density on the wollastonite surfaces related to the nucleation density on calcite plus anorthite. Between the latter two minerals no significant preference for any surface was observed. Random heterogeneous nucleation on all three reactants would lead to a value of 1 in this diagram. During the first 24 hours, nucleation on wollastonite surfaces was preferred by a factor of 12. Over the first 48 hours nucleation on wollastonite surfaces was preferred by a factor of 7 and over longer reaction times (>48 h) by a factor of 3 ± 1. Due to the nucleation rate maximum on the second day, the total population of grossular crystals

TABLE 6

The amount of produced grossular in 5 experiments at 730°C, the measures of the crystals, numbers of crystals, and nucleation rates

Experiment	**G 74**	**G 67**	**G 48**	**G 52**	**G 27**
Duration [h]	24	48	73	120	239
Conversion [%]	2	7	12	16	ca. 27
CO_2(prod.) [mg]	0.06	0.16	0.26	0.36	ca. 0.59
gro (prod.) [mg]	0.60	1.62	2.65	3.64	ca. 5.89
V_{gro} [cm^3]	0.20×10^{-3}	0.54×10^{-3}	0.88×10^{-3}	1.21×10^{-3}	ca. 1.96×10^{-3}
V[cm^3]	9.0×10^{-3}	8.7×10^{-3}	8.3×10^{-3}	8.1×10^{-3}	7.5×10^{-3}
A_{gro} per cm^3 [cm^2]	50.5	214.0	346.8	455.1	765.3
$\overline{D_x}$ [μm]	20.9 ± 0.6	11.1 ± 0.3	12.6 ± 0.3	14.6 ± 0.3	13.7 ± 0.4
$\overline{A_x}$ [μm^2]	1628 ± 87	506 ± 29	641 ± 31	832 ± 36	743 ± 38
$\overline{V_x}$ [μm^3]	7088 ± 550	1464 ± 188	1959 ± 155	2748 ± 200	2552 ± 204
N_{gro}	0.28×10^5	3.69×10^5	4.50×10^5	4.41×10^5	7.69×10^5
$N_{V,gro}$ [cm^{-3}]	0.31×10^7	4.23×10^7	5.41×10^7	5.47×10^7	10.3×10^7
R_n[$cm^{-3} \times sec^{-1}$]	36	>454	131	≈ 66	≈ 66

V_{gro} = volume of produced grossular
V = volume of the solid reaction mixture after reaction
A_{gro} per cm^3 = total surface area of the grossular crystals per 1 cm^3 of solid reaction mixture
$\bar{D}_x$ = mean diameter of the grossular crystals
$\bar{A}_x$ = mean surface area of the grossular crystals
$\bar{V}_x$ = mean volume of the grossular crystals
N_{gro} = number of grossular crystals formed in the run
$N_{V,gro}$ = number of grossular crystals formed per 1 cm^3 of solid reaction mixture
R_n = integrated nucleation rate, i.e. the number of grossular crystals formed in 1 cm^3 of solid reaction mixture per 1 second.

is dominated by these crystals, so that the preference of 3 ± 1 is consistent with random nucleation in the time interval after the nucleation rate maximum.

Crystal growth rates.—The mean diameter, $\bar{D}_x$, surface area, $\bar{A}_x$, and volume, $\bar{V}_x$, of the grossular crystals formed in the five runs at 730°C were calculated from the measured size distributions, approximating the crystals as spheres. It is obvious from the crystal size histograms (fig. 9) that a large shift in mean diameters occurs between 24 and 48 hours with the largest mean diameter being present after 24 hours ($\bar{D}_x$ = 20.9 μm), and the smallest after 48 hours ($\bar{D}_x$ =11.1 μm) (table 6). This behavior is reflected in figure 12 where the mean crystal volume over the entire grossular population, $\bar{V}_x$, is compared to the mean volume of the crystals growing on wollastonite

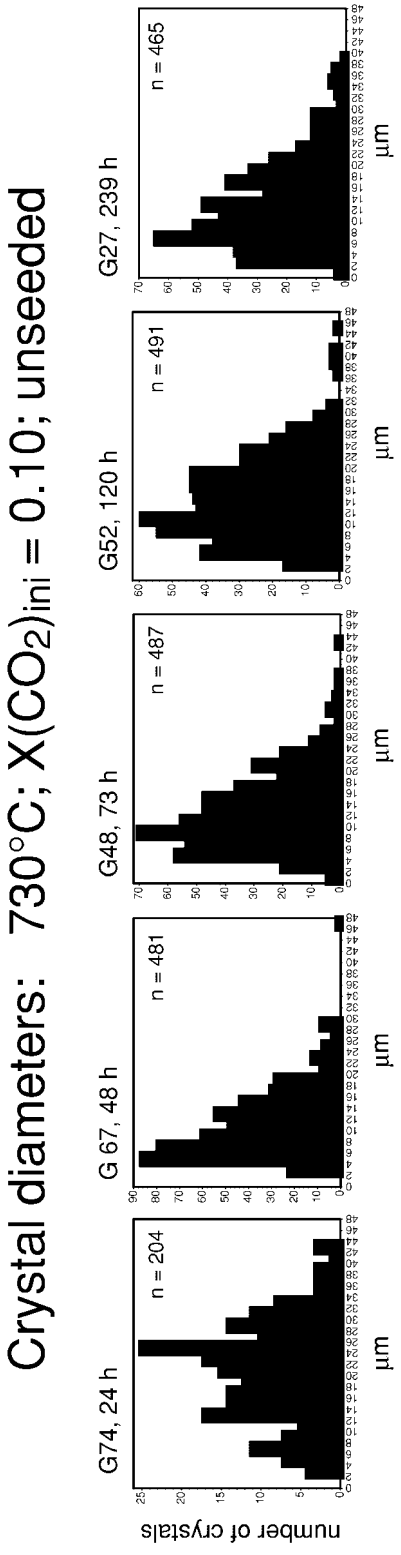

Fig. 9. Crystal size distributions (CSD) of five experiments at 730°C. Note that the scale of the ordinate is different in the single histograms.

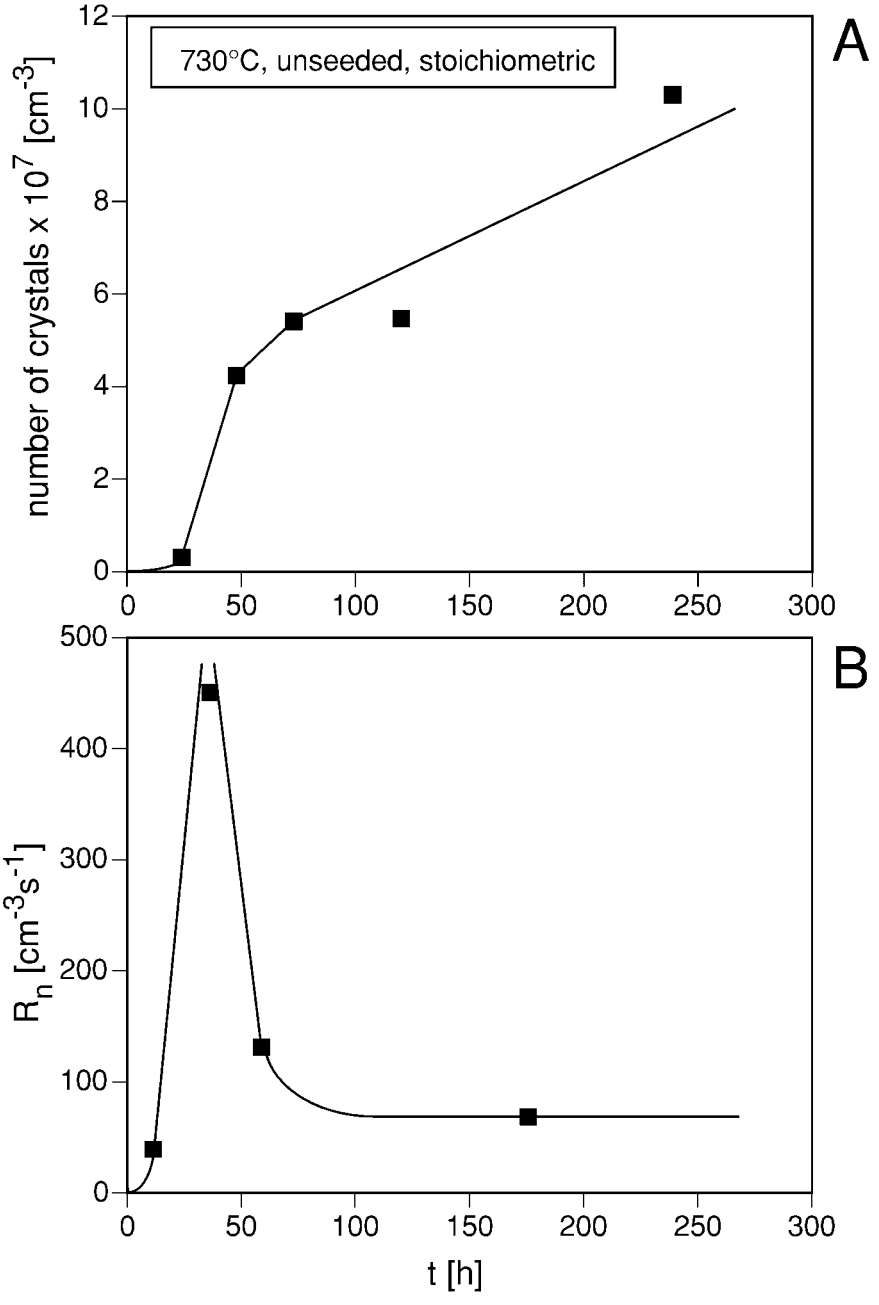

Fig. 10. (A) Number of grossular crystals per cubic centimeter of solid phases, $N_{V,gro}$, versus time (730°C; $X(CO_2)_{ini}$ = 0.10; stoichiometric; unseeded). (B) Integrated nucleation rate, R_n, versus time, as derived from the increasing number of crystals.

surfaces. $\bar{V}_x$ varies between 7090 μm^3 (after 24 h) and 1460 μm^3 (after 48 h). After this minimum at 48 hours, there was a slow increase of mean crystal volumes. There is practically no difference between the sub-population growing on wollastonite and the total population. Thus, the nucleation substrate has no effect on the growth rates.

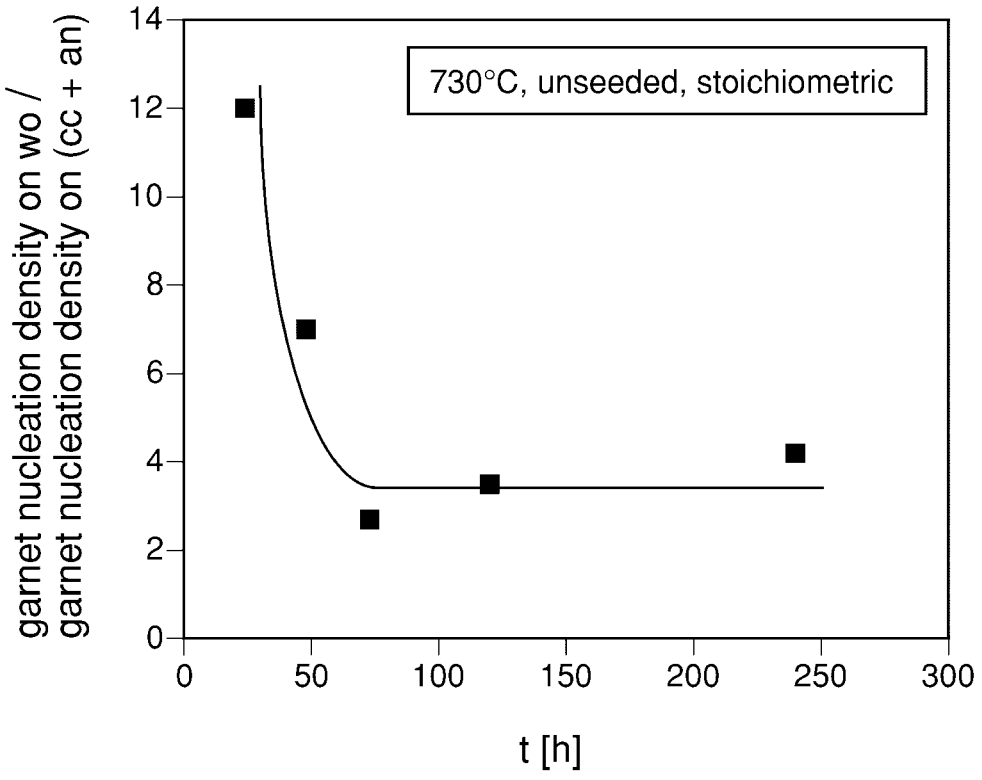

Fig. 11. Garnet nucleation density on wollastonite surfaces divided by nucleation density on calcite + anorthite surfaces versus time from the 5 experiments at 730°C.

Multiplying the number of grossular crystals, $N_{V,gro}$, with their mean surface area, $\bar{A}_X$, the evolution of the total grossular surface area, A_{gro}, over the course of the reaction is obtained. A_{gro} (normalized to 1 cm^3 of solids) is listed in table 6 and depicted as a function of time in figure 13. It increases from 51 cm^2 at 24 hours to 765 cm^2 at 239 hours. The most prominent increase of about 6.0 cm^2/h occurs between 24 and 73 hours and reflects the nucleation rate maximum.

Mean crystal growth rates for partial populations of the garnet crystals were derived by a statistical method described in Appendix B. The method is based on the assumption that the later nucleating crystals do not grow faster than the already present crystals (either with respect to their diameters, surface areas, or volumes, depending on the type of growth rate law), so that early nucleated crystals are always larger than later nucleated crystals. Crystal growth rates were statistically derived for the two partial populations of crystals that nucleated during the first 24 hours of the runs ($t_{nuc} \leq 24$ h) and those that nucleated during the second 24 hour interval (24 h $< t_{nuc} \leq 48$ h) (fig. 14 and table 7). The crystals of both partial populations grew steadily. In both groups the growth rates decreased with time, either with regard to diameter, surface area, or volume. The mean diameter of the group $t_{nuc} \leq 24$ h increased from 20.9 μm at 24 hours to 34.4 μm at 239 hours. The crystals of the group 24 h $< t_{nuc} \leq$ 48 h grew from μm at 48 hours to 19.9 μm at 239 hours. There is a constant difference of 15 ± 0.5 μm between both groups.

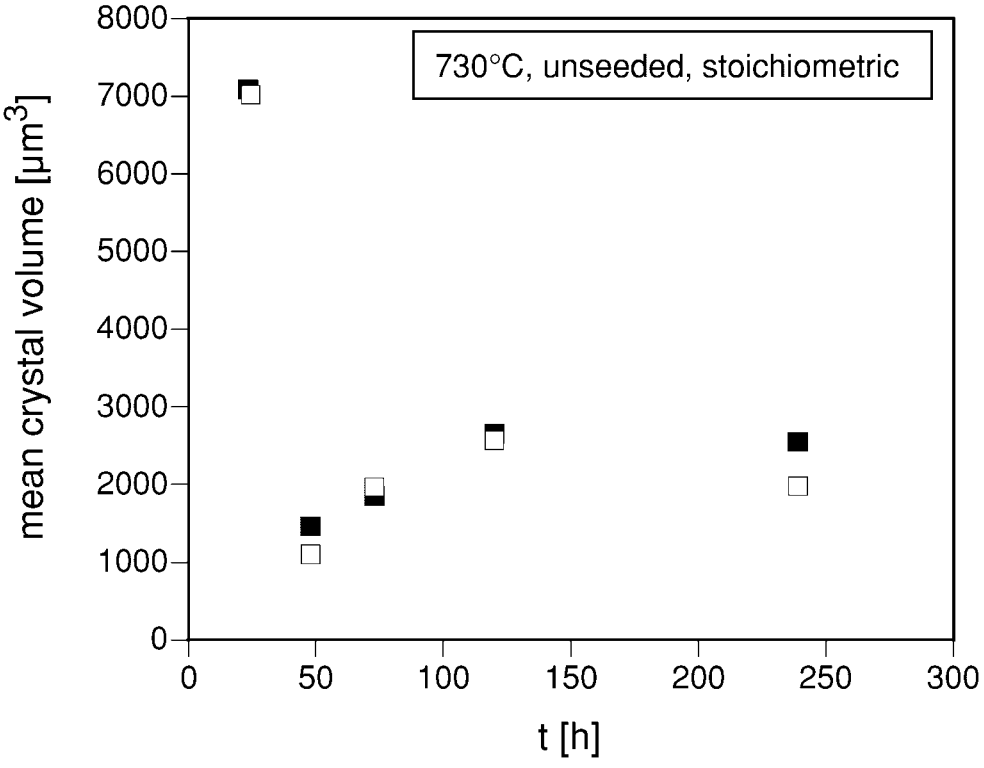

Fig. 12. Mean volume of grossular crystals versus time in the five experiments at 730°C. All measured crystals (filled squares); crystals on wollastonite surfaces (open squares).

DISCUSSION

Rate-limiting step.—In order to understand the kinetics of a reaction, the first aim is to identify the rate-limiting step. In a serial reaction mechanism, the slowest step in a chain of steps controls the overall reaction rate, whereas in a parallel reaction mechanism the slowest step on the fastest path is rate-controlling (Lasaga, 1998). The rate-controlling step can change several times during the course of a reaction (Lüttge and Metz, 1991). It is important to note that there is not always a single rate-controlling step in mineral reactions. Although long established (Burke, 1965; Lasaga, 1986), this fact is often ignored. Burke (1965; p. 31–32) demonstrated the absence of a single rate-limiting step by a simple flow-through model, where the total flow is constrained by the flow rates through two orifices which are not independent from each other and thus are both, in a way, 'rate-limiting'. Translated to mineral reactions, this analogy means that a single rate-controlling step only exists if it is much slower than all the other steps and its rate is independent of the other reaction steps. Consider a model reaction A + B + C = D + E. Dissolution of phase A is the rate-controlling step, if phase A dissolves much slower than B and C, if the dissolution reactions of B and C do not affect the dissolution rate of phase A, and if dissolution is slower than the transport and growth steps in this reaction. However, if two or more reactants supply the same chemical species, their dissolution reactions might mutually affect each other. If phase A is one of the reactants, this interference amongst chemical species in solution will be of little importance as long as the concentrations of the dissolved species in the fluid

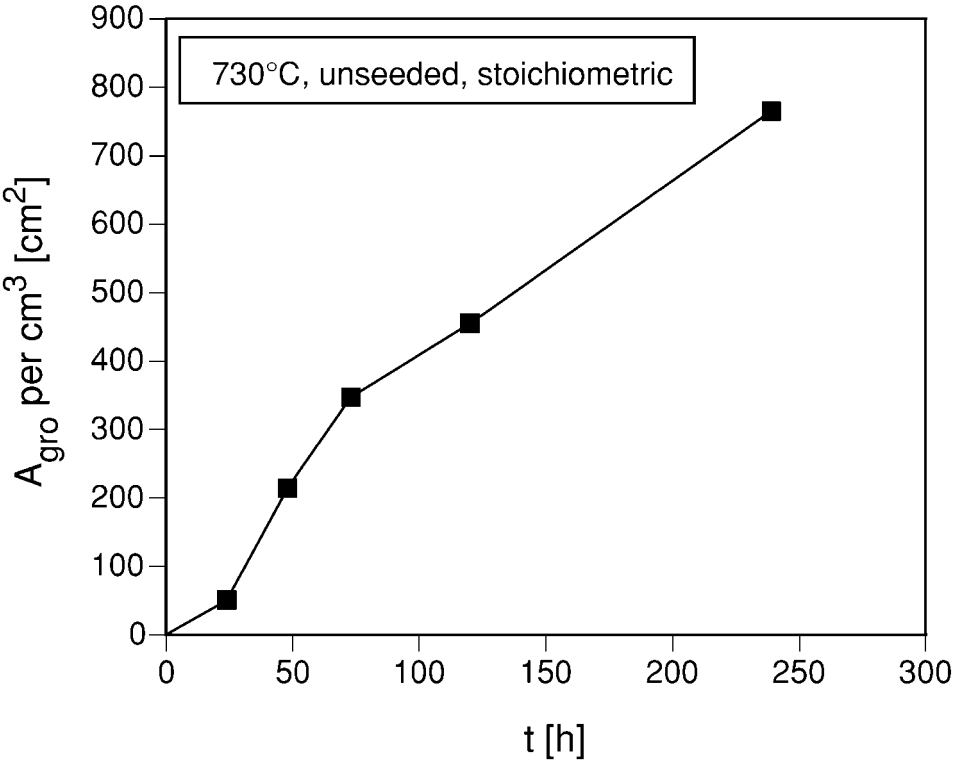

Fig. 13. Grossular surface area versus time in the five experiments at 730°C.

are low; but chemical interferences will become increasingly important the more the dissolved species approach concentrations in equilibrium with phase A.

In many experimental studies on heterogeneous reactions of petrologic relevance, the kinetics have been interpreted in terms of serial reaction mechanisms. Both dissolution or crystallization steps were identified as being rate limiting, so that the reaction rates are linearly related to the surface area of one rate-controlling phase (Matthews, 1985; Schramke and others, 1987; Dachs and Metz, 1988; Ostapenko and others, 1991, 1992). This scenario is true as long as product minerals do not armor the reactants. If armoring occurs, the surface area of one or more phases in contact with the fluid could diminish, and the dissolution of these phases could become rate limiting (Lüttge and Metz, 1991; Winkler and Lüttge, 1999).

In our study, there is no explicit relationship between the surface area of any reactant and the reaction rate. The experiments with increased surface area, due to either smaller grains or a surplus of one reactant, lead to diametrical results. In contrast, the seeded experiments show a correlation between reaction rates and the amount of grossular in the starting mixtures. The positive relationship between the amount of grossular seeds and the reaction rate (fig. 8) suggests that reaction rates are a function of the grossular surface area and that grossular crystallization controls the overall reaction rate. However, there are several arguments against this interpretation.

If the reaction rate were indeed controlled by the grossular surface area, A_{gro}, the reaction would accelerate according to the increase in A_{gro}. For example, at 730°C A_{gro} increased by a factor of 3 from the second to the fifth day of the reaction (fig. 13).

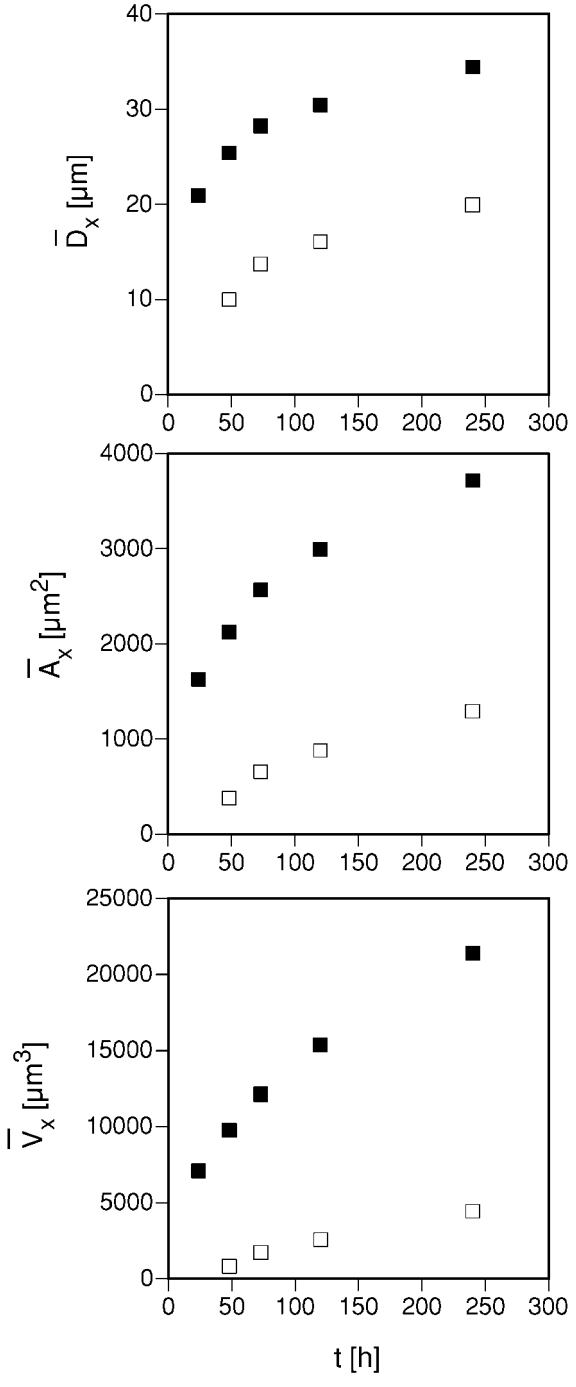

Fig. 14. Mean diameter ($\bar{D}_x$), mean surface area ($\bar{A}_x$), and mean volume ($\bar{V}_x$) of grossular crystals versus time in the five experiments at 730°C. Sub-population $t_{nuc} \leq 24$ hours (filled squares), sub-population 24 hours $< t_{nuc} \leq 48$ hours (open squares).

TABLE 7

Mean grossular diameters ($\bar{D}_x$), surface areas ($\bar{A}_x$), and volumes ($\bar{V}_x$) for the two partial populations of grossular crystals that nucleated during the first 24 hours of the runs and during the time span from 24–48 hours, respectively

run No.	run duration y [h]	n_y	$t_{nuc} \leq 24$ h				$24h < t_{nuc} \leq 48h$			
			$n_{nuc}^{\leq 24h}$	$\bar{D}_x$ [μm]	$\bar{A}_x$ [μm^2]	$\bar{V}_x$ [μm^3]	$n_{nuc}^{24h<t\leq 48h}$	$\bar{D}_x$ [μm]	$\bar{A}_x$ [μm^2]	$\bar{V}_x$ [μm^3]
G74	**24 h**	204	204	20.89 ± 0.63	1628 ± 87	7088 ± 550	-	-	-	-
G67	**48 h**	481	35	25.42 ± 0.95	2126 ± 215	9748 ± 2087	446	9.99 ± 0.22	379 ± 15	814 ± 46
G48	**73 h**	487	28	28.26 ± 0.82	2568 ± 164	12126 ± 1377	353	13.72 ± 0.24	657 ± 23	1720 ± 89
G52	**120 h**	491	28	30.45 ± 0.99	2997 ± 212	15355 ± 1914	352	16.06 ± 0.25	879 ± 27	2554 ± 115
G27	**239 h**	465	14	34.43 ± 0.65	3718 ± 139	21399 ± 1227	177	19.91 ± 0.32	1293 ± 43	4426 ± 232

t_{nuc} = time of nucleation

n_y = number of measured crystals in the experiment of duration y

$n_{nuc}^{\leq 24h}$ = number of crystals that nucleated during the first 24 hours of the runs, calculated using eq (A7)

$n_{nuc}^{24h<t\leq 48h}$ = number of crystals that nucleated during the time span from 24–48 hours, calculated using eq (A8). Example: in the 48 hour experiment 35 out of the 481 measured crystals nucleated during the first 24 hours. They are the 35 largest crystals in this run. The mean diameter, $\bar{D}_x$, of these 35 crystals is 25.4 μm. In the 73 hour run (G67) 28 out of the 487 measured crystals nucleated during the first 24 hours. They are the 28 largest crystals in the run. Their mean diameter is 28.3 μm. 353 out of the 487 crystals have nucleated during the time span from 24 to 48 h. Their $\bar{D}_x$ of 13,7 μm is the mean diameter of the 353 crystals following in size behind the 28 largest crystals.

However, the reaction rate remained constant. In order to compensate for a three-fold increase in surface area, the temperature overstepping must have strongly decreased. As the mean overstepping during the second day was about 68°C, overstepping would have to have been reduced to about 40°C (as extrapolated from fig. 4), tantamount to a shift in $X(CO_2)$ of 0.121, a CO_2 production of 0.67 mg and a conversion of 31 percent. However, the measured reaction progress after 5 days at 730°C was less than 20 percent (G37, G52, G94; fig. 3). Surface-controlled kinetics as a function of the grossular surface area therefore does not agree with the linear reaction rate curves.

The same result is obtained if we compare the reaction progress in the reheating experiment with the seeded runs (fig. 7). At the first and second reheating, the amount of grossular in the capsule was 0.53 and 1.88 mg, respectively. Seeding with that same amount of added seeds would lead to twofold and six fold increases in the reaction rates, respectively. However, in the reheating experiment the reaction rate was the same as in the uninterrupted standard experiments and did not change after the reheating steps. This absence of reaction enhancement shows that the rate-increasing effect in the seeded experiments was caused by a factor other than the increase in the grossular surface area.

A third argument is based on the crystal growth rate curves (fig. 14). The crystals grew by spiral growth (fig. 2H). If a surface reaction step controlled their growth rates, the measured rates would have to fit a rate law for spiral growth. The periodic bond chain theory (PBC theory) of crystal growth predicts linear increase of crystal diameter as a function of ΔG for conditions far from equilibrium and as a function of ΔG^2 near equilibrium (see for example, Lasaga, 1998). Several experimental studies have found that crystal growth rates are a function of ΔT^2 (Lasaga, 1998). If the growth rates were controlled by spiral growth, the consecutive crystal growth rates could be extrapolated from the rates between 24 and 48 hours, approximating ΔG as being proportional to ΔT (= temperature overstepping, $T - T_{eq}$). This extrapolation is shown in figure 15 for the two boundary cases, "growth rate $\propto \Delta T$" and "growth rate $\propto \Delta T^2$", in comparison to the measured diameters of the sub-population $t_{nuc} \leq 24$ hours. The measured decrease in growth rates is neither proportional to ΔT or ΔT^2, but much stronger. Thus, if crystal growth rates were surface-controlled, the crystals should have grown much faster in the time period after more than 48 hours. This conclusion again implies that another factor, different from a surface reaction on the grossular surfaces, limits the overall reaction rates and again confirms that the grossular surface area cannot be rate-controlling.

It follows from the above arguments that the overall reaction rates are not a function of any reactant or product surface area. Moreover, there is no rimming of reactants by grossular and none of the reactants is overgrown and isolated from the fluid to a significant extent. From the crystal size distributions (fig. 9) and the nucleation densities (fig. 11) it can be calculated, that not more than 5 percent of the wollastonite surface area was covered by grossular crystals after 24 hours and not more than 18 percent after 48 hours (at 730°C). Calcite and anorthite are overgrown to an even smaller extent. Although there is no single rate-limiting step, the reaction rates change in response to different variations of the starting conditions. These differences include variations in surface areas; numbers of grains; fluid-solid ratio and so forth. Apparently, in any of these situations, the system adjusts to a different steady state level by the interplay of several reaction steps.

The question remains why the reaction wollastonite + anorthite + calcite = grossular + CO_2 is controlled by a combination of reaction steps, whereas the kinetics of many other mineral reactions under similar experimental conditions can be successfully explained by a single rate-controlling step. In the studied reaction, interference between several dissolution reactions is favored by the fact that Si-species

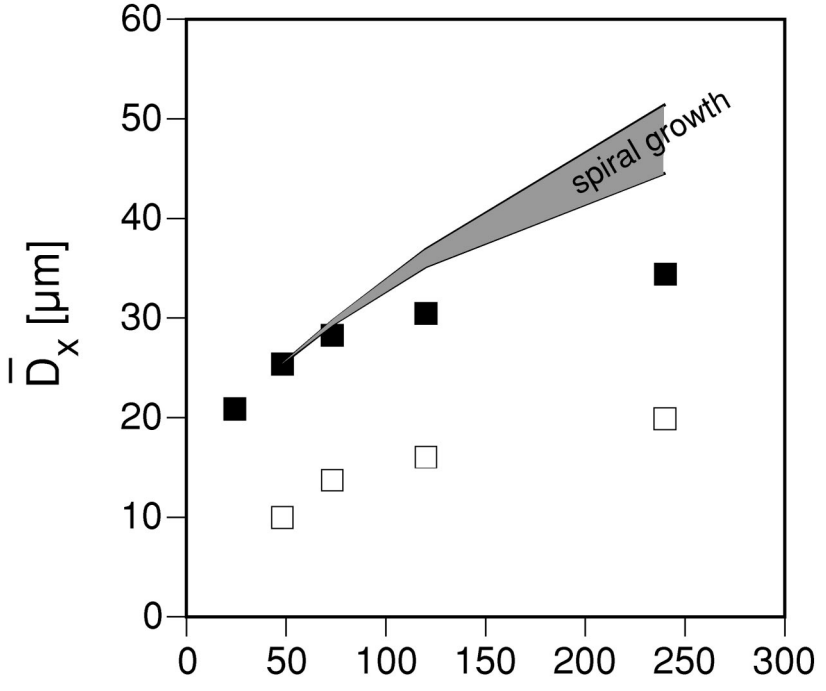

Fig. 15. Mean diameter ($\bar{D}_x$) of grossular crystals versus time from figure 14 together with modeled growth curves assuming the growth rates were controlled by spiral growth (shaded area; the lower curve is for "rate $\propto \Delta T$" and the upper curve for "rate $\propto \Delta(T^2)$"). The model curves are projected from the measured growth rate between 24 and 48 hours.

are supplied by both anorthite and wollastonite, and Ca-species are supplied by calcite, anorthite, and wollastonite. Both anorthite and wollastonite dissolve very fast (Lasaga, 1984), such that high concentrations of dissolved species in the fluid are reached after a short run time. Additionally, wollastonite represents an extreme case of incongruent dissolution, including the formation of a Ca-depleted surface layer (Casey and others, 1993; Xie and Walther, 1994). It is possible that, at the temperatures of these experiments, anorthite dissolves incongruently as well. SEM observations of crystallographically controlled dissolution of calcite and wollastonite indicate that they were only weakly undersaturated in the fluid. This fact implies that concentrations of Ca- and Si-species must have been high. Weak undersaturation is strongly implied by the evolution of flat crystal faces from the broken ends of wollastonite prisms in experiments at 700°C and below. Although wollastonite morphologically appears to have been a reaction product, grossular formation in the same experiments clearly indicates that wollastonite was consumed as a reactant.

Microsystems.—The spatial arrangements of reactant and grossular grains have an impact on the reaction rates. This conclusion follows from a comparison of the experiments where the surface area of one reactant was doubled by a surplus or by smaller grains, and also by comparison of the seeded runs with the reheated capsules in the reheating experiment. In both cases, the charges are identical in mass and composition, but differ in the spatial arrangement of the grains. Thus, certain arrangements of grains, or microsystems, in the reactant mixtures seem to favor grossular formation. The availability of such microsystems determines the reaction rates. Characteristics of these microsystems can be deduced from the experimental results.

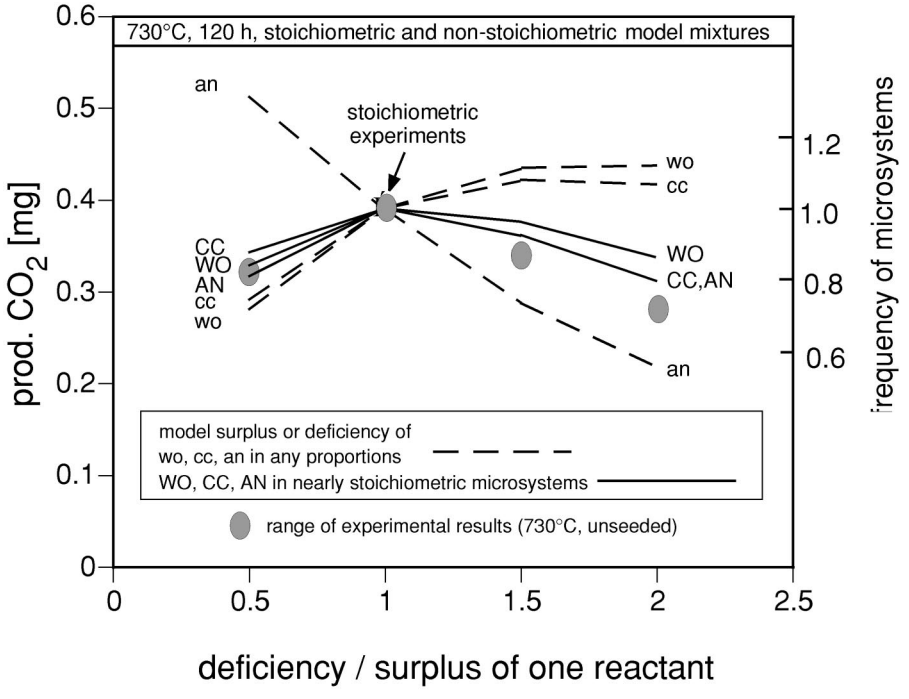

Fig. 16. Conversion (produced CO_2) in stoichiometric and non-stoichiometric experiments for 120 hours at 730°C from figures 3 and 6 (grey shaded areas). Overlain is the calculated frequency of microsystems where all three reactants meet in arbitrary proportions (dashed lines) and where the three crystals meet in proportions similar to the stoichiometric proportions (solid lines). Both are normalized to the frequency of the respective microsystems in the stoichiometric mixture.

In the seeded experiments, the grossular seed crystals were randomly distributed throughout the capsules. Seeding led to higher reaction rates compared to unseeded runs and the reheating experiment. An explanation for the slower reaction rates in the reheating experiment could be that the distribution of grossular crystals, the sites of heterogeneous nucleation, were not random, but confined to favored microsystems where their subsequent growth caused them to ultimately interfere with each other. The nature of these microsystems is indicated by the experiments with surplus or deficiency of one reactant. In these cases, the reaction rates were maximized in stoichiometric mixtures (fig. 6), that is, where the number of local grain arrangements reflecting stoichiometric composition occurred with the highest frequency. A close relationship exists between the frequency of stoichiometrically composed microsystems and reaction rates, as shown by a frequency calculation of such microsystems (Appendix C; fig. 16). From this observation we conclude that the favored sites for grossular growth are wollastonite grain surfaces situated within a local arrangement of stoichiometrical composition relevant to the grossular-forming reaction.

The evolution of chemically distinct microsystems is not unique to the studied reaction, even under fluid-rich experimental conditions comparable to our runs. Lüttge and others (1996) studied the reaction 1 tremolite + 11 dolomite = 8 forsterite + 13 calcite + 9 CO_2 + 1 H_2O. They identified distinct compositions of fluid inclusions trapped in forsterite and related them to different microenvironments. In the same reaction, Heinrich and others (1986, 1989) observed dissolution embayments surrounding forsterite crystals on dolomite surfaces, similar to the dissolution

embayments in our experiments. Such embayments form by locally enhanced dissolution in the near vicinity of the growing crystals and therefore are direct evidence for steep concentration gradients in the fluid phase.

These dissolution embayments merit special notice. They indicate that there is a positive feedback between localized dissolution and growth. In material science, and recently also in the geological literature, this localized mutual interplay is denoted as autocatalysis. Autocatalysis generally occurs when a reactant phase is situated within the diffusion distance of a product phase (Anderson and others, 1998a, b). Autocatalysis has been described in mineral reactions between carbonates, for example precipitation of cerussite on phosgenite surfaces (Pina and others, 2000) and between phosphates, for example precipitation of xenotime and monazite on apatite grain surfaces and within apatite grains (Harlov and others, 2002). An important aspect of autocatalytic reactions is the absence of a single rate-limiting step, as dissolution and crystallization rates are not independent from each other. As evident from the dissolution embayments, the studied grossular-forming reaction is autocatalytic as well during the early stages of the experiments.

According to this model, the grossular crystals are surrounded by spherical halos where concentrations of dissolved species are lower than in the 'bulk' fluid. The diameters of these halos can be estimated by analogy to the thickness of the diffusion boundary layers in aqueous fluids. These layers are usually between 50 and 100 μm thick (see for example, Anderson and others, 1998a). Diffusion gradients made visible by interference microscopy of aqueous solutions surrounding fast growing dendritic crystals (Raz and others, 1989) are of the same order of magnitude. If the favored nucleation sites are randomly distributed in the reactant mixtures, it can be calculated at which point in time the diffusion halos totally fill the inner volume of the capsules, such that they must impinge during subsequent growth. The capsule volume under run conditions is the sum of the fluid and the solid volumes. Using the modified Redlich-Quong-equation (Kerrick and Jacobs, 1981), the density of an H_2O-CO_2-fluid with 10 mole percent CO_2 at 730°C and 400 MPa is 0.67 g/cm^3, such that 12.7 mg of fluid has a volume of 19.0 mm^3. Applying a mean density of 2.7 for the solid mixture, the solids have a volume of 9.4 mm^3. The capsule volume under run conditions thus is 19.0 mm^3 + 9.4 mm^3 = 28.4 mm^3 = 2.84×10^{10} μm^3. Using N_{gro}^{24h} from the experiments at 730°C (table 6) and assuming a halo diameter of 100 μm, the total volume of the diffusion spheres after 24 hours was 1.47×10^{10} μm^3. This value is within one order of magnitude of the capsule volume. It is therefore reasonable that impingement of the reaction halos occurred after about one day in the experiments. This result is in perfect agreement with our measurements of nucleation rates; with the observed crystal growth rates; and with our observations of dissolution embayments. During the second day the nucleation and growth rates strongly decreased and the dissolution embayments disappeared. This behavior indicates that the localized diffusion gradients were leveled.

Overcoming the nucleation barrier.—Andradite-rich cores were found in crystals of all sizes, suggesting that through the entire course of the experiment the crystals nucleate and begin to grow as andradite-rich grandite. At 710°C, iron-rich cores were found in most crystals and, taking sectioning effects into account, are probably present in all of them. At 750°C a larger fraction of crystals had no iron-rich cores. This observation suggests, that at 710°C the critical super-saturation for nucleation of pure grossular was never reached and nucleation only occurred via andradite-rich grandite. At 750°C the nucleation barrier was possibly overstepped, but only for a short period of time. However, once small crystals existed they continued growing as grossular with only 'bulk' Fe concentration. Thus during the entire reaction, small, Fe-rich crystals nucleated and grew between the larger, Fe-poor crystals. Apparently, pure grossular

crystals were not stable in contact with the fluid as long as they had not exceeded a critical size (<5 μm).

Despite the low iron concentrations in the reactants and accordingly in the fluid phase, there is no indication that the substrate preference for grandite nucleation was determined by the availability of iron. There is no preferred nucleation on anorthite surfaces (0.48 wt percent FeO), and wollastonite surfaces (0.39 wt percent FeO) were only preferred in the early stage of the reaction. This early preference for wollastonite is probably related to the initial incongruent dissolution of wollastonite and not to the iron content.

In contrast, iron-enrichment in the garnet cores plays a prominent role for the temporal progression of nucleation. Heterogeneous reactions are characterized by a sequence of stages. These stages include an induction phase before nucleation starts; a nucleation phase with simultaneous nucleation and growth; and a growth phase, in which the supersaturation falls below the nucleation threshold (for example, Lüttge and Metz, 1991). By numerical modeling of the temporal evolution of nucleation rates in a heterogeneous reaction, Lüttge and others (1998) proposed a sharp nucleation rate peak early in the reaction, followed by a long period of continued growth below the nucleation threshold. This peak is similar to the garnet nucleation rate maximum on the second day of our experiments at 730°C. However, in contrast to the model of Lüttge and others (1998), nucleation in our experiments continues at a steady state rate after the nucleation rate maximum. This continuing nucleation also contradicts models for competitive diffusion-controlled growth (Carlson, 1989, 1991). Here depletion halos around the growing crystals are assumed. This process is analogous to the proposed diffusion spheres in our experiments. Once the depletion halos have coalesced, nucleation is expected to totally cease (Carlson, 1991). Thus, if our experiments were subject to similar conditions, there should be no nucleation after the nucleation rate maximum. The continuing nucleation in our experiments may easily be explained by the role of iron. Because the crystals nucleate as andradite-rich grandites below the nucleation threshold of pure grossular, nucleation is not totally suppressed in the diffusion spheres of the grossular crystals.

Implications for experimental and field kinetic studies.—This study points out some pitfalls in experimental kinetic studies. The rates of the studied reaction are not controlled by a single rate-limiting step, but by interplay of various steps. This result is different from the result of numerous reactions studied in powder experiments under pressures and temperatures relevant to metamorphism. In these experiments typically surface-controlled kinetics were found, unless the reactants became totally covered by product rims and diffusion through these rims became rate-limiting (Kridelbaugh, 1973; Tanner and others, 1985; Lüttge and Metz, 1993; Milke and others, 2001; Milke and Heinrich, in press). In the seeded experiments the rates of the studied reaction appeared to be a function of the grossular surface area. However, the detailed data available on nucleation rates, growth rates, and the evolution of the grossular surface area in our experiments prohibits the conclusion that grossular growth is the rate limiting step of the reaction. The correlation between reaction rate and amount of grossular seeds could be identified as misleading as the amount of kinetic data acquired in this study was considerably larger than in previous studies. It is possible that the studied reaction is unique in this respect because of its complexity. This conclusion however, is not certain.

As there is no single rate-limiting step, it does not make sense to normalize the measured reaction rates to any physical value, such as the surface area of either a reactant or the product phase. Consequently, the experimentally determined reaction

rates cannot be directly linked to grossular formation during metamorphism. The same restriction holds true for any other mineral reaction as long as the rate-limiting step is not unambiguously determined.

An important observation in our experiments is the nucleation mechanism via enrichment of iron traces in the garnet crystal cores. A similar observation was made by Lüttge and Neumann (1993), who found several wt percent of silver-aegirine component in the core regions of diopside crystals synthesized by the reaction dolomite + quartz = diopside + carbon dioxide. The silver came from the silver oxalate that was used to produce the H_2O-CO_2 fluid phase and the Fe^{3+} from oxidized trace amounts of FeO in the dolomite. Analog nucleation mechanisms might be common in experiments where impure natural minerals are used as starting materials. They might be even more important in metamorphism where a variety of trace elements typically are present.

This nucleation mechanism could be distinct from the common growth zoning in metamorphic minerals, as for example spessartine-rich cores in almandine-rich garnets or andradite-rich cores in grandites. Apparently chemically homogeneous crystals may well have grown around very small cores of different composition. This nucleation mechanism would have a strong impact on the spatial distribution of crystals and the nucleation rates and would not easily be recognized in natural porphyroblasts if micron-sized nucleation cores are present as in our experiments. The observed nucleation mechanism could not only be relevant to garnet formation, but to many other metamorphic minerals as well. For example, similar to the grandite series, enrichment of iron traces could possibly trigger the nucleation of epidotes. Manganese traces could trigger the nucleation of pyralspite garnets. Candidates for possible nucleation via 'exotic' components can be found in many solid solution series where certain trace elements are preferentially partitioned into the lattice, for example, Zn, Co, and Cr in staurolite, or Cr, V, or Pb in epidotes. Thermodynamic properties of many of these 'exotic' components are undetermined. Nucleation via trace element enrichment during metamorphic crystallization may constitute an effective mechanism to overcome nucleation barriers.

Nucleation normally is suppressed at some point during a mineral reaction, either because supersaturation in the fluid falls below the nucleation threshold or because depletion halos around the growing crystals overlap. However, nucleation via trace element enrichment is still possible and should be represented in crystal size distributions (CSD). Carlson and others (1995) formulated 3-dimensional numerical models for diffusion-controlled nucleation and growth. They calculated the theoretical evolution of porphyroblast populations and then compared the calculated CSDs with measured CSDs from garnetiferous rocks from diverse metamorphic environments. Their model CSDs closely matched the measured ones, though most of the measured CSDs were more positively skewed. Carlson and others (1995) ascribed these deviations in skewedness to kinetic factors not encompassed within their model. They suggested increasing heating rates or initial inhomogeneities in the distribution of the nutrients as possible reasons. Ongoing nucleation after the impingement of depletion halos would also lead to an increasing number of small crystals, that is, positively skewed CSDs, and should therefore be considered in models for diffusion-controlled nucleation and growth.

ACKNOWLEDGMENTS

We thank A. Lüttge, H. W. Day, and C. T. Foster for their elaborate reviews that significantly improved the paper. Thanks to H. Heinrich for reading and commenting on an earlier version of the manuscript. D. E. Harlov is thanked for linguistic improvements. We are also grateful to J. Widmer, U. Winkler, M. Gottschalk, U.

Neumann, and C. Ballhaus for their support and helpful discussions in various stages of the study. We thank M. Hertel for manifold technical assistance, H. Hüttemann for taking the SEM photomicrographs, E. Eipper for assistance at the microprobe, and J. Mällich for preparatory work.

APPENDIX A

Grossular Nucleation Rates

Nucleation rates for grossular are derived by combining the measured crystal size distributions (CSD) with the measured conversions. CSDs were determined from measuring crystal diameters, D_x, using SEM microphotographs. Crystal surface areas, A_x, and volumes, V_x, were calculated using D_x and approximating the grossular crystals as spheres. The volume of grossular produced in an experiment is:

$$V_{gro} = \frac{m_{re} \times \xi \times 0.91}{\rho_{gro}} \tag{A1}$$

where: m_{re} = mass of reactants in a run; ξ = mole fraction of reactants transformed into grossular; ρ_{gro} = density of grossular. The factor 0.91 takes into account the loss of 9.1 wt percent of the reactants as CO_2.

The number of crystals formed in a particular run was calculated from the total grossular volume, V_{gro}, by dividing through the mean crystal volume:

$$N_{gro} = \frac{V_{gro}}{\bar{V}_x} \tag{A2}$$

with: N_{gro} = number of grossular crystals; V_{gro} = total grossular volume formed in an experiment; and $\bar{V}_x$ = mean volume of grossular crystals.

The mean volume of the grossular crystals was directly derived from the CSDs in the reaction mixture of each run by:

$$\bar{V}_x = \frac{\sum_{1}^{n} (V_x \times k)}{n} \tag{A3}$$

with V_x = crystal volume; k = correction factor ($0 < k \leq 1$), taking into account the "missing" volume in the case of intergrown crystals and individually determined for each garnet crystal while measuring its diameter; and n = number of measured crystals per run.

The numbers of crystals were related to a unity volume to make the results of different experiments comparable. As a unity volume, 1 cm^3 of the solid reaction mixture was chosen (consisting of the remaining calcite, wollastonite, and anorthite plus the newly formed grossular). The number of crystals per unity volume is:

$$\frac{N_{gro}}{V} = N_{V,gro} \tag{A4}$$

with: V = volume of the solid reaction mixture in units of cm^3; and $N_{V,gro}$ = number of grossular crystals in 1 cm^3 of the solid reaction mixture.

As a volume reduction of the solids (= 29 percent at 100 percent conversion) must be considered, V can be found using the following relation:

$$V = (1 - \xi) \times \left(\frac{m_{cc}}{\rho_{cc}} + \frac{m_{wo}}{\rho_{wo}} + \frac{m_{an}}{\rho_{an}} \right) + \xi \times \frac{m_{gro}}{\rho_{gro}} \tag{A5}$$

where: m_{cc}, m_{wo}, and m_{an} are the masses of calcite, wollastonite, and anorthite in the starting mixture. m_{gro} = mass of grossular formed when the conversion of the reaction is 100 percent, that is $\xi = 1$.

Nucleation rates are derived from the difference in $N_{V,gro}$ in runs of different duration. If the run time of two experiments differs by Δt, the integrated nucleation rate, R_n, for the time interval Δt is:

$$\frac{N_{V,gro}(t_2) - N_{V,gro}(t_1)}{\Delta t} = R_n \tag{A6}$$

APPENDIX B

Growth Rates of Grossular

As it is not possible to observe grossular growth in our experiments *in situ*, the following statistical method was developed to calculate growth rates. By this method mean growth rates for sub-populations could be derived from the CSDs of the 730°C experiments. The method is based on the assumption, that later nucleating crystals do not grow faster than the already present crystals, such that earlier nucleated crystals are always larger than the later nucleated ones.

The total grossular population was divided up into the following two sub-populations: (1) crystals that nucleated within the first 24 hour interval; their nucleation period is $t_{nuc} \leq 24$ hours; (2) crystals that nucleated within the second 24 hour interval; their nucleation period is $24\ h < t_{nuc} \leq 48$ hours.

After more than 48 hours, the grossular crystals of both groups are growing continuously while new crystals nucleate and grow. Thus, in the runs longer than 48 hours, the crystals from the first 24 hours comprise the fraction of the largest crystals of the CSD. The crystals that nucleated between 24 and 48 hours are smaller than the first group, but larger than all other crystals that nucleated later than 48 hours. The number of crystals belonging to the first group ($t_{nuc} \leq 24$ h) was calculated using equation (A7) and then separated from the upper end of the measured CSDs.

In a run of time y (for example, 48 h) the number of crystals nucleated during the first 24 hours and selected for our statistical evaluation is given by:

$$n_y^{t_{nuc} \leq 24h} = \frac{N_{V,gro24h}}{N_{V,gro,y}} \times n_y \tag{A7}$$

where: n_y = number of the measured crystals in the run of time y.

In the same way all crystals that nucleated during the first 48 hours can be determined from the crystal population of a longer run by:

$$n_y^{t_{nuc} \leq 48h} = \frac{N_{V,gro,48h}}{N_{V,gro,y}} \times n_y \tag{A8}$$

To select the crystals that nucleated in the time interval $24\ \text{hours} < t_{nuc} \leq 48$ hours, the crystals formed in the first 24 hours have to be subtracted. Thus, in a run of time y the crystals that nucleated in the interval from 24 to 48 hours are given by:

$$n_y^{24h < t_{nuc} \leq 48h} = \left(\frac{N_{V,gro,48h}}{N_{V,gro,y}} - \frac{N_{V,gro,24h}}{N_{V,gro,y}} \right) \times n_y \tag{A9}$$

where: $n_y^{24h < t_{nuc} \leq 48h}$ = number of crystals that nucleated in the interval from 24 to 48 h in a run of time y.

The corresponding number of crystals for each group was separated from the CSDs and their mean sizes $\bar{D}_x$, $\bar{A}_x$, and $\bar{V}_x$ were calculated. An example of this calculation is given in the caption of table 7.

APPENDIX C

Frequency Calculation for Stoichiometric and Non-Stoichiometric Microsystem

The reactant mixture was geometrically approximated as cubic close packing of wollastonite, calcite, and anorthite spheres. The tetrahedral and octahedral sites of the package represent the potential sites of grossular crystallization between the reactant grains.

Two cases were considered:

I. The probability that all three reactants meet at a tetrahedral or octahedral site.

II. The probability that all three meet in proportions similar to the stoichiometric proportions relevant to the studied reaction.

The probability calculation is formulated for a mixture of n phases M_i ($i = 1 \ldots n$). m_i is the proportion of grains of M_i in the mixture. x is the number of grains meeting at a potential crystallization site, thus $x = 4$ for tetrahedral sites and $x = 6$ for octahedral sites.

I. The three reactants meet in arbitrary proportions.—The probability, P, that a given grain in the mixture is a grain of M_i is

$$P(M_i) = \frac{m_i}{\sum_{i=1}^{n} m_i} \tag{A10}$$

and the probability that it is not a grain of M_i is

$$\bar{P}(M_i) = 1 - \frac{m_i}{\sum_{i=1}^{n} m_i} \tag{A11}$$

The probability that the phase M_1 is present among the x grains meeting at a potential crystallization site is

$$P_L(M_1) = 1 - [\bar{P}(M_1)]^x \tag{A12}$$

If one of the x grains is a grain of phase M_1, there are $x - 1$ positions left. The probability that one of these $x - 1$ grains is a grain of phase M_2 is

$$P_L(M_2) = 1 - [\bar{P}(M_2)]^{x-1} \tag{A13}$$

Accordingly, in a mixture of n phases, the probability that one of the grains around a potential crystallization site is a grain of the phase M_n is

$$P_L(M_n) = 1 - [\bar{P}(M_n)]^{x-(n-1)} \tag{A14}$$

The probability that all three reactants in the studied reaction mixture meet at a potential crystallization site is

$$P_{1\ldots n} = \prod_{i=1}^{n} P_L(M_i) \tag{A15}$$

II. The three reactants meet in proportions similar to the stoichiometric proportions.—The molar proportions in a stoichiometric mixture are 1 Wo : 1 Cc : 3 An. If the grains were equally sized spheres, the grain proportions were 1 Wo : 1.09 Cc : 2.73 An. Thus, both at tetrahedral and octahedral sites the three reactants could not meet in exactly stoichiometric proportions. For the calculation the arrangement 1 Wo : 1 Cc : 2 An at a tetrahedral site and the arrangement 1 Wo : 1 Cc : 4 An at an octahedral site was considered stoichiometric. The probabilities are summed up over both tetrahedral and octahedral sites. Thus, the systematic errors induced by the deviations from the stoichiometric proportions in part eliminate each other. The probability that exactly one grain around a potential crystallization site is a grain of phase M_1 is given by the probability for the presence of M_1 at this site, multiplied by the number of grains meeting there and the probability that none of the other grains makes up phase M_1:

$$P_{L,M_1,1} = P(M_1) \cdot x \cdot \bar{P}(M_1)^{x-1} \tag{A16}$$

If exactly one grain is a grain of M_1, the probability that *exactly one* of the other grains is made up of M_2 is

$$P_{L,M_2,1} = \frac{m_2}{\sum_{i=2}^{n} m_i} \cdot (x-1) \cdot \left(1 - \frac{m_2}{\sum_{i=2}^{n} m_i}\right)^{x-2} \tag{A17}$$

As there are three reactant phases in the studied reaction, the number of grains of phase M_3 at a potential crystallization site is given as soon as the exact numbers of grains of M_1 and M_2 are defined. Thus, $P_{L,M_3,x-2} = 1$.

The probability that the three reactants meet at a potential crystallization site in proportions similar to the stoichiometric proportions is

$$P_{1,2,3,st} = \prod_{i=1}^{n-1} P_{L,M_i} \tag{A18}$$

The table gives the proportions of grains, m_i, of the three reactants in the starting mixtures where one reactant was deficient or in excess.

	stoich	0.5 wo	1.5 wo	2 wo	0.5 cc	1.5 cc	2 cc	0.5 an	1.5 an	2 an
m_{wo}	1	1	1	1	1	1	1	1	1	1
m_{cc}	1.09	2.20	0.73	0.55	0.55	1.65	2.20	1.10	1.10	1.10
m_{an}	2.73	5.46	1.82	1.37	2.73	2.73	2.73	1.37	4.10	5.46

References

Allen, J. M., and Fawcett, J. J., 1982, Zoisite-Anorthite-Calcite stability relations in H_2O-CO_2 fluids at 5000 bars: an experimental and SEM study: Journal of Petrology, v. 23, p. 215–239.

Anderson, J. G., Doraiswamy, L. K., and Larson, M. A., 1998a, Microphase-assisted "autocatalysis" in a solid-liquid reaction with a precipitating product—I. Theory: Chemical Engineering Science, v. 53, p. 2451–2458.

Anderson, J. G., Larson, M. A., and Doraiswamy, L. K., 1998b, Microphase-assisted "autocatalysis" in a solid-liquid reaction with a precipitating product—II. Experimental: Chemical Engineering Science, v. 53, p. 2459–2468.

Burke, J., 1965, The kinetics of phase transformations in metals: Oxford, Pergamon Press, p 226.

Carlson, W. D., 1989, The significance of intergranular diffusion to the mechanisms and kinetics of porphyroblast crystallization: Contributions to Mineralogy and Petrology, v. 103, p. 1–24.

——— 1991, Competitive diffusion-controlled growth of porphyroblasts: Mineralogical Magazine, v. 55, p. 317–330.

Carlson, W. D., Denison, C., and Ketcham, R. A., 1995, Controls on the nucleation and growth of porphyroblasts; kinetics from natural textures and numerical models: Geology Journal, v. 30, p. 207–225.

Casey, W. H., Westrich, H. R., Banfield, J. F., Ferruzzi, G., and Arnold, G. F., 1993, Leaching and reconstruction at the surfaces of dissolving chain-silicate minerals: Nature, v. 366, p. 253–256.

Cashman, K. V., and Ferry, J. M., 1988, Crystal size distribution (CSD) in rocks and the kinetics and dynamics of crystallization III. Metamorphic crystallization: Contributions to Mineralogy and Petrology, v. 99, p. 401–415.

Chernoff, C. B., and Carlson, W. D., 1997, Disequilibrium for Ca during growth of pelitic garnet: Journal of Metamorphic Geology, v. 15, p. 421–438.

Dachs, E., and Metz, P., 1988, The mechanism of the reaction 1 tremolite + 3 calcite + 2 quartz = 5 diopside + 3 CO_2 + 1 H_2O: results of powder experiments: Contributions to Mineralogy and Petrology, v. 100, p. 542–551.

Daniel, C. G., and Spear, F. S., 1999, The clustered nucleation and growth processes of garnet in regional metamorphic rocks from north-west Connecticut, USA: Journal of Metamorphic Geology, v. 17, p. 503–520.

Denison, C., and Carlson, W.D., 1997a, Three-dimensional quantitative textural analysis of metamorphic rocks using high-resolution computed X-ray tomography. Part II: Application to natural samples: Journal of Metamorphic Geology, v. 15, p. 45–57.

——— 1997b, Disequilibrium for Ca during growth of pelitic garnet: Journal of Metamorphic Geology, v. 15, p. 421–438.

Edmunds, W. M., and Atherton, M. P., 1971, Polymetamorphic evolution of garnet in the Fanad aureole, Donegal, Eire: Lithos, v. 4, p. 147–161.

Galwey, A. K., and Jones, K. A., 1963, An attempt to determine the mechanism of a natural mineral-forming reaction from examination of the products: Journal of the Chemical Society, Dalton Transactions, p. 5681–5686.

——— 1966, Crystal size frequency distribution of garnets in some analyzed metamorphic rocks from Mallaig, Inverness, Scotland: Geological Magazine, v. 103, p. 143–152.

Gottschalk, M., 1997, Internally consistent thermodynamic data for rock forming minerals in the system SiO_2—TiO_2—Al_2O_3—Fe_2O_3—CaO—MgO—FeO—K_2O—Na_2O—H_2O—CO_2: European Journal of Mineralogy, v. 9, p. 175–223.

Harlov, D.E., Förster, H-J., and Nijland, T.G., 2002, Fluid induced nucleation of (Y + REE)-phosphate minerals in apatite: nature and experiment Part I. Chlorapatite: American Mineralogist, v. 87, p. 245–261.

Heinrich, W., Metz, P., and Bayh, W., 1986, Experimental investigation of the mechanism of the reaction: 1 tremolite + 11 dolomite = 8 forsterite + 13 calcite + 9 CO_2 + 1 H_2O: Contributions to Mineralogy and Petrology, v. 93, p. 215–221.

Heinrich, W., Metz, P., and Gottschalk, M., 1989, Experimental investigation of the kinetics of the reaction 1 tremolite + 11 dolomite ⇔ 8 forsterite + 13 calcite + 9 CO_2 + 1 H_2O: Contributions to Mineralogy and Petrology, v. 102, p. 163–173.

Huckenholz, H.G., and Fehr, K.T., 1982, Stability relationships of grossular + quartz + wollastonite + anorthite II. The effect of grandite-hydrograndite solid solution: Neues Jahrbuch für Mineralogie Abhandlungen, v. 145, p. 1–33.

Jones, K. A., and Galwey, A. K., 1966, Size distribution, composition, and growth kinetics of garnet crystals in some metamorphic rocks from the west of Ireland: Quarterly Journal of the Geological Society of London, v. 122, p. 29–44.

Kerrick, D. M., and Jacobs, G. K., 1981, A modified Redlich-Kwong equation for H_2O, CO_2, and H_2O-CO_2 mixtures at elevated pressures and temperatures: American Journal of Science, v. 281, p. 735–767.

Kretz, R., 1966, Grain size distribution for certain metamorphic minerals in relation to nucleation and growth: Journal of Geology, v. 74, p. 147–173.
——— 1973, Kinetics of the crystallization of garnet at two localities near Yellowknife: Canadian Mineralogist, v. 12, p. 1–20.
——— 1974, Some models for the rate of crystallization of garnet in metamorphic rocks: Lithos, v. 7, p. 123–131.
——— 1993, A garnet population in Yellowknife schist, Canada: Journal of Metamorphic Geology, v. 11, p. 101–120.
Kridelbaugh, S. J., 1973, The kinetics of the reaction: calcite + quartz = wollastonite + carbon dioxide at elevated temperatures and pressures: American Journal of Science, v. 273, p. 757–777.
Lasaga, A. C., 1984, Chemical kinetics of water-rock interactions: Journal of Geophysical Research, v. 89, B6, p. 4009–4025.
——— 1986, Metamorphic reaction rate laws and development of isograds: Mineralogical Magazine, v. 50, p. 359–373.
——— 1998, Kinetic Theory in the Earth Sciences: New Jersey, Princeton University Press, 811 p.
Lasaga, A. C., Lüttge, A., Rye, D. M., and Bolton, E. W., 2000, Dynamic treatment of invariant and univariant reactions in metamorphic systems: American Journal of Science, v. 300, p. 173–221.
Lasaga, A. C., Rye, D. M., Lüttge, A., and Bolton, E. W., 2001, Calculation of fluid fluxes in Earth's crust: Geochimica. et Cosmochimica Acta, v. 65, p. 1161–1185.
Liu, M., Peterson, J. C., and Yund, R. A., 1997, Diffusion-controlled growth of albite and pyroxene reaction rims: Contributions to Mineralogy and Petrology, v. 126, p. 217–223.
Lüttge, A., and Metz, P., 1991, Mechanism and kinetics of the reaction 1 dolomite + 2 quartz = 1 diopside + 2 CO_2 investigated by powder experiments: Canadian Mineralogist, v. 29, p. 803–821.
——— 1993, The mechanism and kinetics of the reaction 1 dolomite + 2 quartz = 1 diopside + 2 CO_2; a comparison of rock-sample and of powder experiments: Contributions to Mineralogy and Petrology, v. 115, p. 155–164.
Lüttge, A., and Neumann, U., 1993, Side reactions: An experimental study of metastable phase formation: Terra abstracts 5/1, 354
Lüttge, A., Metz, P., Walther, J., Althaus, E., and Heinrich, W., 1996, CO_2-H_2O fluid inclusions in forsterite: An experimental study: European Journal of Mineralogy, v. 8, p. 997–1014.
Lüttge, A., Neumann, U., and Lasaga, A.C., 1998, The influence of heating rate on the kinetics of mineral reactions: An experimental study and computer models: American Mineralogist, v. 83, p. 501–515.
Matthews, A., 1985, Kinetics and mechanisms of the reaction of zoisite to anorthite under hydrothermal conditions: reaction phenomenology away from the equilibrium region: Contributions to Mineralogy and Petrology, v. 89, p. 110–121
Matthews, A., and Goldsmith, J. R., 1984, The influence of metastability on reaction kinetics involving zoisite formation from anorthite at elevated pressures and temperatures: American Mineralogist, v. 69, p. 848–857.
Milke, R., and Heinrich, W., 2002, Diffusion-controlled growth of wollastonite rims between quartz and calcite: Comparison between nature and experiment: Journal of Metamorphic Geology, in press.
Milke, R., Wiedenbeck, M., and Heinrich, W., 2001, Grain boundary diffusion of Si, Mg, and O in enstatite reaction rims: a SIMS study using isotopically doped reactants: Contributions to Mineralogy and Petrology, v. 142, p. 15–26.
Ostapenko, G. T., Gorogotskaya, L. I., and Timoshkova, L. P., 1991, Sillimanite-kyanite conversion kinetics: Geochemistry International, v. 28, p. 79–85.
Ostapenko, G. T., Gorogotskaya, L. I., Timoshkova, L. P., and Chibisov, A. I., 1992, Kyanite → andalusite, kyanite → sillimanite, and andalusite → sillimanite transformation kinetics: Geochemistry International, v. 29, p. 1–10.
Pina, C. M., Fernández-Diaz, L., Prieto, M., and Putnis, A., 2000, *In situ* atomic force microscope observations of a dissolution-crystallisation reaction: The phosgenite-cerussite transformation: Geochimica et Cosmochimica Acta, v. 64, p. 215–221.
Raz, E., Lipson, S. G., and Polturak, E., 1989, Dendritic growth of ammonium chloride crystals: Measurements of the concentration field and a proposed nucleation model for growth: Physical Review, v. A 40, p. 1088–1095.
Schramke, J. A., Kerrick, D. M., and Lasaga, A. C., 1987, The reaction muscovite + quartz = andalusite + K-feldspar + water. Part 1. Growth kinetics and mechanism: American Journal of Science, v. 287, p. 517–559.
Skelton, A.D.L., 1997, The effect of metamorphic fluid flow on the nucleation and growth of garnets from Troms, North Norway: Journal of Metamorphic Geology, v. 15, p. 85–92.
Tanner, S. B., Kerrick, D. M., and Lasaga, A. C., 1985, Experimental kinetic study of the reaction: calcite + quartz = wollastonite + carbon dioxide, from 1 to 3 kilobars and 500° to 800°C: American Journal of Science, v. 285, p. 577–620.
Winkler, U., and Lüttge, A., 1999, The influence of $CaCl_2$ on the kinetics of the reaction 1 tremolite + 3 calcite + 2 quartz = 5 diopside + 3 CO_2 + 1 H_2O. An experimental investigation: American Journal of Science, v. 299, p. 393–427.
Yund, R. A., 1997, Rates of grain boundary diffusion through enstatite and forsterite reaction rims: Contributions to Mineralogy and Petrology, v. 126, p. 224–236.
Xie, Z., and Walther, J. V., 1994, Dissolution stoichiometry and adsorption of alkali and alkaline earth elements to the acid-reacted wollastonite surface at 25°C: Geochimica et Cosmochimica Acta, v. 58, p. 2587–2598.